# Explicit Hilbert-space representations of atomic and molecular photoabsorption spectra: Computational studies of Stieltjes-Tchebycheff functions

M. R. Hermann and P. W. Langhoff
*Department of Chemistry,* Indiana University, Bloomington, Indiana 47405*
*and Max Planck Institut für Astrophysik, Karl-Schwarzschild-Strasse 1, D-8046 Garching bei München, Federal Republic of Germany*
(Received 16 December 1982)

Explicit Hilbert-space techniques are reported for construction of the discrete and continuum Schrödinger states required in atomic and molecular photoexcitation and/or photoionization studies. These developments extend and clarify previously described moment-theory methods for determinations of photoabsorption cross sections from discrete basis-set calculations to include explicit construction of underlying wave functions. The appropriate Stieltjes-Tchebycheff excitation and ionization functions of $n$th order are defined as Radau-type eigenstates of an appropriate operator in an $n$-term Cauchy-Lanczos basis. The energies of these states are the Radau quadrature points of the photoabsorption cross section, and their (reciprocal) norms provide the corresponding quadrature weights. Although finite-order Stieltjes-Tchebycheff functions are $L^2$ integrable, and do not have asymptotic spatial tails in the continuous spectrum, the Radau quadrature weights nevertheless provide information for normalization in the conventional Dirac $\delta$-function sense. Since one Radau point can be placed anywhere in the spectrum, appropriately normalized convergent approximations to any of the discrete or continuum Schrödinger states are obtained from the development. Connections with matrix partitioning methods are established, demonstrating that $n$th-order Stieltjes-Tchebycheff functions are optical-potential solutions of the matrix Schrödinger equation in the full Cauchy-Lanczos basis. The energies at which the $n$th-order optical potential vanishes identically correspond to generalized Gaussian quadrature points, in which case the associated Stieltjes eigenfunctions provide an optimal $L^2$ representation of the Schrödinger spectrum of discrete and continuum wave functions. The spectral contributions of individual Schrödinger states to $n$th-order Stieltjes-Tchebycheff functions are obtained in closed form, indicating the latter are spectrally localized in the neighborhoods of the Radau quadrature energies, and spatially localized in accordance with the extent of the target eigenstate. Illustrative studies of the dipole spectra in atomic and molecular hydrogen clarify the nature and convergence of the method. Finally, procedures are indicated for construction of photoemission anisotropies and for performing coupled-channel calculations employing Stieltjes-Tchebycheff functions, and descriptive intercomparisons are made of the present development with more conventional computational procedures.

## I. INTRODUCTION

Continuing refinements in experimental studies of molecular vacuum uv photoionization cross sections and of corresponding photoejection angular distributions employing line-source,[1] synchrotron-radiation,[2] and equivalent-photon $(e,2e)$ electron coincidence[3] techniques have been reported in the recent literature.[4] Correspondingly, computational approximations to the associated theoretical expressions for partial cross sections and anisotropy factors have provided useful clarification of the measured results in many instances.[5] One of the computational methods currently employed, the so-called Stieltjes-Tchebycheff moment-theory approach,[6] makes use of the familiar discrete-basis-set methodology of bound-state studies, and, consequently, is applicable in a convenient manner to the noncentral and nonlocal potentials that arise in molecular body-frame calculations.[7] This approach has proved useful for computations of partial-channel cross sections in the static-exchange approximation for a number of molecules,[8] and furnishes a natural setting for discussion of the shape resonances that arise in short bond length molecules from $\sigma^*$ orbitals in photoionization continua.[9] Further refinement and clarification of the approach seems desirable, however, in view of continuing interest in molecular ionization spectroscopy. Of particular value would be studies of the wave functions underlying the method,[10] and indication of their connection with the scattering functions of conventional single-center approaches, which are generally written in angular momentum representation.[11] Moreover, prescriptions for calculations of molecular anisotropy factors from the continuum functions,[12] and further elaboration of applications in coupled-channel situations would also be helpful.[13]

In this paper, the $L^2$ Stieltjes-Tchebycheff functions that underlie the moment approach to molecular photoabsorption and ionization studies are indicated,[9,10] some of their properties are described, and computational applications are reported. Tchebycheff functions of $n$th order are defined, in accordance with previously described (Tchebycheff) approximations to spectral densities,[14] as $L^2$ eigen-

 

functions of an appropriate operator in an $n$-term Cauchy-moment basis set.[10] Their energies are the Radau quadrature points of the photoabsorption cross section, and their norms are seen to provide the corresponding quadrature weights.[15] Although Tchebycheff functions do not have asymptotic spatial parts in finite orders, they nevertheless provide the information required for normalization in the Dirac $\delta$-function sense. Since one Radau point can be placed anywhere in the spectrum, the Tchebycheff development provides appropriately normalized $L^2$ approximations to discrete and continuum molecular eigenfunctions at any energy. Connections are made with matrix partitioning methods,[16] which show that the Tchebycheff functions are optical-potential solutions of the full Schrödinger problem in the complete Cauchy-moment basis.[17] Stieltjes functions of $n$th order are seen to provide a special set of $L^2$ eigenstates having energies at which the optical potential vanishes identically. These energies are the generalized Gaussian quadrature points of the density, with the (reciprocal) norms of the Stieltjes functions providing the corresponding quadrature weights.[15] Because Gaussian quadrature points are sure to appear where the defining density is large, the corresponding Stieltjes functions provide an optimal $L^2$ representation of the spectrum; i.e., they are the natural pseudostates of the system.[10] The Stieltjes-Tchebycheff functions can be regarded as $L^2$ packets or spectral integrals over the correct Schrödinger states in the neighborhoods of the Radau or Gaussian quadrature energies. It is shown that the spectral contribution of an individual discrete or continuum Schrödinger state to a Stieltjes-Tchebycheff function can be evaluated in closed form without explicit reference to or construction of the correct Schrödinger wave functions. In the limit of high order, the Stieltjes-Tchebycheff functions are seen to converge to appropriately normalized discrete and continuum Schrödinger states,[18] whereas in finite orders they provide accurate approximations to Schrödinger states over predetermined finite spatial intervals.

Detailed illustrative applications of the development are provided in the cases of atomic and molecular hydrogen. Stable recursive Lanczos methods are employed in construction of invariant Cauchy subspaces of specific order,[19] and in determinations of corresponding recurrence coefficients for orthogonal polynomials required in the development.[15] Since the energy dependence of the Stieltjes-Tchebycheff functions appears only in recursively defined orthogonal polynomials, their construction is particularly rapid and efficient once the Cauchy-Lanczos basis has been determined. In atomic hydrogen, all quantities necessary for construction of regular $l$-wave spectra are obtained in closed form, and detailed computational results in high order are reported for the dipole or ($l=1$) $p$-wave spectrum. Calculations in molecular hydrogen are reported in the static-exchange approximation for $1\sigma_g \rightarrow k\sigma_u$ and $k\pi_u$ excitation and/or ionization symmetries in the body frame. Very large Cartesian Gaussian basis sets and canonical orthogonalization procedures are used in constructing the Cauchy-Lanczos basis functions in these cases. The resulting Stieltjes-Tchebycheff functions are presented in three-dimensional graphical forms over an appropriate energy range. These are seen to provide useful diagnostics of the corresponding photoionization continua, and, in particular, to clarify the nature of the $\sigma \rightarrow \sigma^*$ transition in $H_2$.[9]

The theoretical development is given in Sec. II and computational results are reported in Sec. III. In Sec. IV, concluding and descriptive remarks of a general nature are made. Advantages and limitations of the Stieltjes-Tchebycheff approach to spectral studies, relative to more conventional discrete and continuum wave-function calculations, are discussed, and aspects of applications of the approach in single-channel approximations to larger molecules are described. Procedures are also indicated for construction of photoejection anisotropies and for performing coupled-channel calculations employing the Stieltjes-Tchebycheff formalism. Finally, explicit descriptive intercomparisons are made of the nature and diagnostic value of Stieltjes-Tchebycheff functions, which are constructed in body-frame point group symmetry in molecular cases, with more conventional scattering functions, which are generally constructed in single-center $l$-wave or eigenchannel representations.

## II. THEORETICAL DEVELOPMENT

In this section, the Schrödinger problem of interest is described, the Cauchy-Lanczos basis and orthonormal polynomials used in constructing $L^2$ Stieltjes-Tchebycheff approximations to the discrete and continuum states are defined, and certain properties of these functions are indicated.

The Schrödinger equation for an individual atom or molecule,

$$(H-\epsilon)\Psi_\epsilon = 0 \ , \tag{1}$$

where $H$ is the appropriate many-electron Hamiltonian, generally gives rise to a denumerably infinite set of bound states as well as an essential spectrum of scattering or ionization states. The bound-state solutions ($\epsilon=\epsilon_i<0$) are made to satisfy physical normalization

$$\langle \Psi_i \mid \Psi_j \rangle = \delta_{ij} \ , \tag{2a}$$

while the scattering states ($\epsilon \geq 0$) satisfy improper or Dirac normalization

$$\langle \Psi_\epsilon \mid \Psi_{\epsilon'} \rangle = \delta(\epsilon-\epsilon') \tag{2b}$$

in the energy variable.[20] The continuous spectrum is furthermore highly degenerate in that all angular momentum waves generally contribute to the wave function at a given energy, and quantization in the direction of outgoing or incoming electrons is also permissible.[20] Moreover, various energetically degenerate channels, corresponding to production of different ionic states, can contribute to the total wave functions at a given energy. In this case, specific boundary conditions must be enforced in order to extract the appropriate physical information.[11] In the present development, attention focuses on single-channel body-frame calculations employing electronic wave functions of good symmetry type. Questions relating to the angular distributions of photoejected electrons, aspects of molecular autoionization, dissociative recombination, and

the general coupled-channel scattering problem are treated separately,[21] although some relevant descriptive remarks are made in Sec. IV below.

Variational approximations to the spectrum of Eq. (1), constructed in finite-dimensional $L^2$ basis sets, are generally regarded as appropriate for the first few bound states of the system.[22] In the present development, it is shown that approximations of uniform quality are obtained to all the discrete and scattering states of Eq. (1) from this familiar computational methodolgy when appropriate procedures are employed. It is important to recognize in this connection that the Schrödinger states of Eq. (1) also satisfy the generalized equation

$$[A(H)-a(\epsilon)]\Psi_\epsilon=0\ , \tag{3}$$

where $A(H)$ is an explicit operator function of the Hamiltonian $H$, and $a(\epsilon)\equiv A(\epsilon)$ gives the corresponding eigenvalues. Equation (3) provides a somewhat more general and flexible basis for introduction of computational approximations than does Eq. (1), as indicated further below.

### A. Many-electron basis sets

The photoabsorption cross section of an atom or molecule is proportional to the squared dipole matrix element

$$g(\epsilon)=|\langle\Psi_\epsilon|\mu|\Psi_0\rangle|^2\ , \tag{4a}$$

where $\Psi_0$ is the target-state eigenfunction of interest, and $\mu$ is a particular polarization component of the dipole operator.[20] It is convenient to regard

$$\Phi\equiv\mu\Psi_0 \tag{4b}$$

as a test function on the spectrum, in accordance with the definition of Eq. (4a). A particularly useful many-electron $L^2$ basis set is generated from $\Phi$ by the prescription[10]

$$\theta_k=[A(H)]^k\Phi,\quad k=0,1,2,\ldots \tag{5}$$

where $A(H)$ is chosen for present purposes to be of the form[23]

$$A(H)\equiv(H-\epsilon_0)^{-1} \tag{6}$$

with $\epsilon_0$ the target-state energy. The metric of this so-called Cauchy-moment basis[10]

$$\begin{aligned}\langle\theta_k|\theta_l\rangle&=\langle\Phi|[A(H)]^{(k+l)}|\Phi\rangle\\&=\int_{-\infty}^{+\infty}[a(\epsilon)]^{(k+l)}g(\epsilon)d\epsilon\\&=\int_{-\infty}^{+\infty}(\epsilon-\epsilon_0)^{-(k+l)}g(\epsilon)d\epsilon\end{aligned} \tag{7}$$

is seen to correspond to reciprocal power moments of the cross section $g(\epsilon)$, which is conveniently regarded as a spectral density having both discrete and continuum parts. Moreover, the operator $A(H)$ in this basis

$$\begin{aligned}\langle\theta_k|A(H)|\theta_l\rangle&=\langle\Phi|[A(H)]^{(k+l+1)}|\Phi\rangle\\&=\int_{-\infty}^{+\infty}[a(\epsilon)]^{(k+l+1)}g(\epsilon)d\epsilon\\&=\int_{-\infty}^{+\infty}(\epsilon-\epsilon_0)^{-(k+l+1)}g(\epsilon)d\epsilon\end{aligned} \tag{8}$$

is evidently also determined by the (reciprocal) spectral power moments. Since the moment integrals of Eqs. (7) and (8) are known to converge to finite values,[20] the $\theta_k$ of Eq. (5) are seen to form a Hilbert space,[10] as indicated above. As a consequence, the eigenvalues and corresponding effective oscillator strengths obtained from the eigenfunctions of $A(H)$ in the Cauchy basis set have certain useful properties discussed previously in considerable detail.[6] In the present development, attention focuses on the eigenfunctions themselves, and on some of their properties. Since $A(H)$ and $H$ have common eigenstates, approximations to the spectrum of the former are, of course, also appropriate for the latter. It should be noted, however, that it is generally not possible to work directly with $H$ in place of $A(H)$ in the development of Eqs. (5)—(8), since positive-integer power moments of the dipole cross section do not converge,[20] and the associated $\theta_k$ functions consequently do not form a Hilbert space.[10]

Use of an $n$-term Cauchy basis and the corresponding matrix elements of Eq. (8) results in an eigenvalue problem that becomes computationally unstable for large $n$.[10] This difficulty is avoided by construction of an orthonormal basis in the $n$-term Cauchy-Hilbert space that brings the matrix representative of the operator $A(H)$ to tridiagonal form. Such Lanczos functions are obtained without explicit reference to the Cauchy basis from the recursive equations[19]

$$\beta_j v_{j+1}=[A(H)-\alpha_j]v_j-\beta_{j-1}v_{j-1},\quad j=1,2,\ldots \tag{9}$$

where ($v_0=0$)

$$v_1=\Phi/\langle\Phi|\Phi\rangle^{1/2}\ , \tag{10a}$$

$$\alpha_j=\langle v_j|A(H)|v_j\rangle\ , \tag{10b}$$

$$\beta_j=\langle v_{j+1}|A(H)|v_j\rangle\ , \tag{10c}$$

$$\langle v_j|v_k\rangle=\delta_{jk}\ , \tag{10d}$$

and $\Phi$ is the test function of Eqs. (4). Equations (9) and (10) provide a complete recursive definition of the Lanczos functions $v_j$, and of the corresponding matrix elements $\alpha_j$ and $\beta_j$, once the test function $\Phi$ is specified. Methods for solution of the Lanczos equations employing $A(H)$ are described in detail in Sec. III.

### B. Schrödinger states

Schrödinger eigenstates in the Lanczos basis are written in the convenient form[24]

$$\Phi_\epsilon=\sum_{j=1}^{\infty}q_j(\epsilon)v_j\ , \tag{11}$$

where the $q_j(\epsilon)$ are elements of the vector representative $\underline{q}_\epsilon$ of the wave function satisfying the Schrödinger problem for $A(H)$ [Eq. (3)],

$$[\underline{A}-a(\epsilon)\underline{I}]\underline{q}_\epsilon=0\ . \tag{12}$$

Here,

$$(\underline{A})_{j,j}=\alpha_j\ , \tag{13a}$$

$$(\underline{A})_{j,j+1}=(\underline{A})_{j+1,j}=\beta_j \tag{13b}$$

is the infinite-order tridiagonal matrix representative of $A(H)$ in the Lanczos basis. Because of the definition of Eqs. (9) and (10), the $\underline{A}$ matrix is of Jacobi form,[24] and the $q_j(\epsilon)$ are found to satisfy the recurrence relation [cf. Eq. (9)]

$$\beta_j q_{j+1}(\epsilon)=[a(\epsilon)-\alpha_j]q_j(\epsilon)-\beta_{j-1}q_{j-1}(\epsilon) \tag{14}$$

with $q_0=0$ and $q_1=1$. The $q_j(\epsilon)$ are orthonormal polynomials satisfying[15]

$$\int_{-\infty}^{+\infty} q_j(\epsilon)q_k(\epsilon)d\Gamma(\epsilon)=\delta_{jk} , \tag{15}$$

where it is convenient to define[23]

$$\begin{aligned} d\Gamma(\epsilon)&=(\,|\,\langle\Psi_\epsilon\,|\,\Phi\rangle\,|^2/\langle\Phi\,|\,\Phi\rangle)d\epsilon \\ &=[g(\epsilon)/\langle\Phi\,|\,\Phi\rangle]d\epsilon . \end{aligned} \tag{16}$$

The (nondecreasing) function $\Gamma(\epsilon)$ is seen to be the distribution corresponding to the (non-negative) spectral density $g(\epsilon)$ of Eq. (4a). Because the operators $A(H)$ and $H$ have the same eigenstates, the solutions of Eqs. (11)—(16) differ from the $\Psi_\epsilon$ of Eq. (1) only by the normalization convention employed. Specifically, using Eq. (15), the $\Phi_\epsilon$ of Eq. (11) are found to satisfy[24]

$$\int_{-\infty}^{+\infty}\langle\Phi_\epsilon\,|\,\Phi_{\epsilon'}\rangle d\Gamma(\epsilon) \;=\int_{-\infty}^{+\infty}\sum_{j=1}^{\infty} q_j(\epsilon)q_j(\epsilon')d\Gamma(\epsilon)=1 \tag{17}$$

for any two points $\epsilon$ and $\epsilon'$ in the spectrum, rather than the conditions of Eqs. (2). Consequently, the distribution $\Gamma(\epsilon)$, which has both continuous and discontinuous parts, is seen to provide the measure according to which the $\Phi_\epsilon$ are normalized.

### C. Stieltjes-Tchebycheff functions

Although the solutions of Eqs. (11) are formally correct,[18] interest centers here on $n$-term approximations to the spectrum. To clarify the natures of such approximations, Eq. (12) is rewritten in the partitioned form[16,17]

$$\begin{bmatrix} \underline{A}^{(n)} & \underline{\beta} \\ \underline{\beta}^\dagger & \underline{R} \end{bmatrix}\begin{bmatrix} \underline{q}_\epsilon^{(n)} \\ \underline{Q}_\epsilon \end{bmatrix}=a(\epsilon)\begin{bmatrix} \underline{q}_\epsilon^{(n)} \\ \underline{Q}_\epsilon \end{bmatrix} , \tag{18}$$

where $\underline{A}^{(n)}$ is $(n\times n)$ tridiagonal, $\underline{\beta}$ has only one nonzero element $(\beta_n)$ in the lower left-hand corner, and $\underline{R}$ is an infinite-order tridiagonal remainder matrix. The finite vector $\underline{q}_\epsilon^{(n)}$ satisfies the optical-potential Schrödinger equation[17]

$$[\underline{A}^{(n)}+\underline{V}^{(n)}(\epsilon)-a(\epsilon)\underline{I}^{(n)}]\underline{q}_\epsilon^{(n)}=0 , \tag{19}$$

where $\underline{V}^{(n)}(\epsilon)$ is given by the formal expression

$$\underline{V}^{(n)}(\epsilon)=\underline{\beta}[\underline{I}a(\epsilon+i0)-\underline{R}]^{-1}\underline{\beta}^\dagger . \tag{20}$$

As a consequence of the definition of the Lanczos basis, it is found that the optical potential of Eq. (20) has only one nonzero element $(n,n)$ given by[25]

$$[\underline{V}^{(n)}(\epsilon)]_{n,n}=-\cfrac{\beta_n^2}{a(\epsilon)-\alpha_{n+1}-\cfrac{\beta_{n+1}^2}{a(\epsilon)-\alpha_{n+2}-\cfrac{\beta_{n+2}^2}{a(\epsilon)-\alpha_{n+3}-\cdots}}} \tag{21a}$$

and that the infinite-order continued fraction of Eq. (21a), when employed in Eq. (19), can be summed to the rational function

$$[\underline{V}^{(n)}(\epsilon)]=\beta_n q_{n+1}(\epsilon)/q_n(\epsilon) \tag{21b}$$

for any energy $\epsilon$ in the Schrödinger spectrum of Eq. (18).[17]

The first $n$ Lanczos functions of Eqs. (9) and (10) are evidently sufficient to determine the optical-potential matrix element of Eqs. (21), in spite of the fact that it corresponds to a closed-form evaluation of the inverse of an infinite-order remainder matrix [Eq. (20)]. Consequently, the $n$-term wave function corresponding to Eq. (19),

$$\Phi_\epsilon^{(n)}=\sum_{j=1}^{n} q_j(\epsilon)v_j , \tag{22}$$

which is seen to be comprised of the first $n$ terms of the correct solutions of Eq. (11), provides an exact optical-potential approximation to the Schrödinger state at energy $\epsilon$. The $n$th-order Stieltjes-Tchebycheff functions of Eq. (22) provide the central computational tool of the present development, and will be seen to furnish accurate approximations to the local portions (in the sense of $\Phi$) of Schrödinger states.

### D. Properties of Stieltjes-Tchebycheff functions

Some of the properties of the Stieltjes-Tchebycheff functions of Eq. (22) are of interest in the present development. These functions are easily constructed once the first $n$ Lanczos functions and related matrix elements $\alpha_j$ and $\beta_j$ are determined from Eqs. (9) and (10), since the corresponding orthogonal polynomials $q_j(\epsilon)$ of Eq. (22) are obtained for any energy $\epsilon$ by recursion using Eq. (14). These polynomials are seen to provide projections of the Lanczos functions

$$\begin{aligned} q_j(\epsilon)&=\langle v_j\,|\,\Phi_\epsilon\rangle \\ &=\langle v_j\,|\,\Phi_\epsilon^{(n)}\rangle \end{aligned} \tag{23}$$

on both the correct Schrödinger states of Eq. (11) and on the $n$th-order Stieltjes-Tchebycheff functions of Eq. (22). Moreover, they are found to be characteristic polynomials of the $n$th-order truncation[26]

$$q_{n+1}(\epsilon)=(-1)^n\det|\,\underline{A}^{(n)}-a(\epsilon)\underline{I}^{(n)}\,|\,\Big/\prod_{i=1}^{n}\beta_i \tag{24}$$

of the $\underline{A}$-matrix Schrödinger equation in the Lanczos basis [Eq. (12)]. Since the optical potential of Eqs. (21) vanishes at the roots of Eq. (24), Eq. (19) reduces to the $n$th-order

truncation of Eq. (12) for these characteristic eigenvalues. The corresponding eigensolutions in this special case are designated Stieltjes eigenfunctions, which provide an optimal $n$-term set of $L^2$ pseudostates for representation of the spectrum,[10] as indicated further below. At the roots of $q_n(\epsilon)$, the optical potential of Eqs. (21) evidently diverges, in which case the $n$ solutions of Eq. (19) include one state having an infinite eigenvalue.

All the solutions of Eq. (19) are included in the simple expression of Eq. (22) as $\epsilon$ is varied over the infinite energy interval $(-\infty,+\infty)$. Although $n$th-order Stieltjes-Tchebycheff functions for two arbitrary energies $\epsilon$ and $\epsilon'$ are not necessarily orthogonal, for any preselected value $\epsilon$ and corresponding function [Eq. (22)] there will be $n-1$ other orthogonal solutions of Eq. (19). The eigenvalues of these orthogonal Tchebycheff eigenfunctions are the roots of the so-called quasiorthogonal polynomials[15]

$$\tilde{q}_{n+1}(\epsilon',\epsilon)\equiv(-1)^n\det|\underline{A}^{(n)}+\underline{V}^{(n)}(\epsilon)-a(\epsilon')\underline{I}^{(n)}|\Big/\prod_{i=1}^{n}\beta_i$$

$$=q_{n+1}(\epsilon')-\frac{q_{n+1}(\epsilon)}{q_n(\epsilon)}q_n(\epsilon')\ , \tag{25}$$

where an expansion in minors has been employed. As indicated above, when $\epsilon$ is set equal to any one of the roots of $q_{n+1}(\epsilon)$ [Eq. (24)], the optical-potential matrix $\underline{V}^{(n)}(\epsilon)$ vanishes, and the $n$ orthogonal Tchebycheff eigenfunctions become $n$th-order Stieltjes eigenfunctions.

The overlap of an arbitrary pair of Stieltjes-Tchebycheff functions is, from Eq. (22),

$$\langle\Phi_\epsilon^{(n)}|\Phi_{\epsilon'}^{(n)}\rangle=\sum_{j=1}^{n}q_j(\epsilon)q_i(\epsilon')$$

$$\equiv K^{(n)}(\epsilon,\epsilon')\ , \tag{26}$$

where $K^{(n)}(\epsilon,\epsilon')$ is termed the polynomial kernel of order $n$.[24] This kernel has the properties[24]

$$K^{(\infty)}(\epsilon,\epsilon')\to<\infty,\quad \epsilon'=\epsilon=\epsilon_i \tag{27a}$$

$$\to\infty,\quad \epsilon'=\epsilon\neq\epsilon_i \tag{27b}$$

$$\to 0,\quad \epsilon'\neq\epsilon \tag{27c}$$

for discrete states ($\epsilon'$ and $\epsilon<0$), and

$$K^{(\infty)}(\epsilon,\epsilon')\to\infty,\quad \epsilon=\epsilon'\geq 0 \tag{27d}$$

$$\to 0,\quad \epsilon\neq\epsilon'\geq 0 \tag{27e}$$

in the essential portion ($\epsilon'$ and $\epsilon>0$) of the spectrum. Moreover, it is seen from Eq. (26) that

$$\int_{-\infty}^{+\infty}\langle\Phi_\epsilon^{(n)}|\Phi_{\epsilon'}^{(n)}\rangle d\Gamma(\epsilon)$$

$$=\int_{-\infty}^{+\infty}\sum_{j=1}^{n}q_j(\epsilon)q_j(\epsilon')d\Gamma(\epsilon)=1\ , \tag{27f}$$

as in Eq. (17) for the converged states ($n\to\infty$). These properties are in accord with the norms of bound and continuum Schrödinger states [Eqs. (1)]. Consequently, physically normalized approximations to Schrödinger states appropriate for the discrete spectral interval are obtained from the Stieltjes-Tchebycheff functions [Eq. (22)] in the form

$$\Psi_\epsilon^{(n)}=[\Gamma^{(n)}(\epsilon)]^{1/2}\sum_{j=1}^{n}q_j(\epsilon)v_j,\quad \epsilon<0 \tag{28a}$$

where

$$\Gamma^{(n)}(\epsilon)=\left[\sum_{j=1}^{n}[q_j(\epsilon)]^2\right]^{-1} \tag{28b}$$

is the Christoffel number or Radau weight at energy $\epsilon<0$.[15] Energy normalized approximations to scattering states are correspondingly obtained from the expression [cf. Eq. (27f)]

$$\Psi_\epsilon^{(n)}=[g^{(n)}(\epsilon)/\langle\Phi|\Phi\rangle]^{1/2}\sum_{j=1}^{n}q_j(\epsilon)v_j\ ,\quad \epsilon\geq 0\ . \tag{29a}$$

Here,

$$g^{(n)}(\epsilon)=\frac{d}{d\epsilon}\left[\tfrac{1}{2}\Gamma^{(n)}(\epsilon)+\sum_i\Gamma_i^{(n)}(\epsilon)\right],\quad \epsilon_i^{(n)}(\epsilon)<\epsilon \tag{29b}$$

is the previously described $n$th-order Stieltjes-Tchebycheff approximation to the density $g(\epsilon)$ of Eq. (4a), obtained as indicated from the derivative of the $n$th-order Radau quadrature approximation $[\epsilon_i^{(n)}(\epsilon),\Gamma_i^{(n)}(\epsilon)]$ to the distribution $\Gamma(\epsilon)$.[14] As discussed earlier,[6-10] in many cases it is preferable to smooth the distribution in Eq. (29b) prior to evaluating the derivative.

The states of Eqs. (28) are clearly unity normalized in each order for any energy $\epsilon<0$. Moreover, in the limit of high order[14]

$$\Gamma^{(\infty)}(\epsilon)\to\sum_{i=1}^{\infty}(|\langle\Psi_i|\Phi\rangle|^2/\langle\Phi|\Phi\rangle)\delta(\epsilon-\epsilon_i),\quad \epsilon<0 \tag{30}$$

so that convergence to the correct discrete spectrum is obtained. Correspondingly, in the essential spectrum it is found from Eqs. (11), (27), and (29) that

$$\langle\Psi_\epsilon^{(\infty)}|\Psi_{\epsilon'}^{(\infty)}\rangle\to\delta(\epsilon-\epsilon')\ , \tag{31}$$

in accordance with convergence to Dirac $\delta$-function normalized scattering states [Eq. (2b)].

In finite orders the functions of Eqs. (28) and (29) provide appropriately normalized approximations to the local portions of discrete and continuum Schrödinger states, as a consequence of the definition and nature of the Cauchy-Lanczos basis. Such localized states can be regarded as spectral averages over the correct Schrödinger functions in the neighborhoods of the chosen energies. It is important to recognize in this connection that the projection of the correct Schrödinger states of Eq. (11) on the Stieltjes-Tchebycheff function of Eq. (22) is obtained in the simple form [cf. Eq. (26)]

$$\langle\Phi_{\epsilon'}|\Phi_\epsilon^{(n)}\rangle=\sum_{j=1}^{n}q_j(\epsilon')q_j(\epsilon)\ . \tag{32}$$

Similar expressions for the physically normalized states

[Eqs. (28) and (29)] are obtained by multiplication of Eq. (32) with the appropriate weight or density factors. The spectral content of Eq. (32) as a function of $\epsilon'$ can be expected to peak in the neighborhood of $\epsilon$, and with increasing $n$ to converge to a $\delta$-function-like structure, in accordance with the convergence of the corresponding Stieltjes-Tchebycheff functions to the correct Schrödinger states.[18]

### E. Connections with moment theory

It is of some interest to make explicit connection between the Stieltjes-Tchebycheff functions of Eq. (22) and previously described moment-theory approximations to spectral densities and distributions.[14] This is accomplished most directly by recalling that the test function $\Phi$ [Eqs. (4)] provides power moments

$$\begin{aligned}\mu_k &= \langle \Phi \mid [A(H)]^k \mid \Phi \rangle / \langle \Phi \mid \Phi \rangle \\ &= \int_{-\infty}^{+\infty} [a(\epsilon)]^k [g(\epsilon)/\langle \Phi \mid \Phi \rangle] d\epsilon \\ &= \int_{-\infty}^{+\infty} (\epsilon - \epsilon_0)^{-k} d\Gamma(\epsilon) \end{aligned} \tag{33}$$

of the density $g(\epsilon)$ [Eqs. (4)]. In previous developments,[6-10] a sequence of $2n-1$ of the moments $\{\mu_k; k=0,1,\ldots,2n-2\}$ are employed in construction of $n$th-order Radau quadrature points and weights in accordance with the moment equations[15]

$$\Gamma^{(n)}(\epsilon)[a(\epsilon)]^k + \sum_{j=1}^{n-1} \Gamma_j^{(n)}(\epsilon)[a_j^{(n)}(\epsilon)]^k = \mu_k \ , \qquad k=0,1,\ldots,2n-2 \ . \tag{34}$$

Here, $\epsilon$ is an arbitrary spectral energy, as in Eq. (22), and $\Gamma^{(n)}(\epsilon)$ is the Radau weight at that point. The latter is obtained from the reciprocal norm of the associated Stieltjes-Tchebycheff function in the form [cf. Eqs. (26) and (28)]

$$\Gamma^{(n)}(\epsilon) = \langle \Phi_\epsilon^{(n)} \mid \Phi_\epsilon^{(n)} \rangle^{-1} \ . \tag{35}$$

Similarly, the $n-1$ other Radau points $a_j^{(n)}(\epsilon)$ are obtained from the eigenvalues of Eq. (25), and the $n-1$ other weights $\Gamma_j^{(n)}(\epsilon)$ are obtained from Eq. (35) with $\epsilon$ replaced by the $\epsilon_j^{(n)}(\epsilon)$. When $\epsilon$ is set equal to one of the roots of Eq. (24), the Radau quadratures of Eq. (34) become generalized Gaussian quadratures that reproduce an additional moment $\mu_{2n-1}$.[14] These correspond to the Stieltjes eigenvalues and eigenfunctions of Eq. (19) with vanishing optical potential.

It is seen that the Stieltjes-Tchebycheff functions of Eq. (22) provide all of the information of the previously described moment-theory developments.[14] In particular, they furnish the quadrature weights for appropriate renormalization [Eqs. (28) and (29)], without reference to the spatially asymptotic portions of scattering functions. Moreover, the intimate connection between orthogonal Tchebycheff eigenfunctions and Radau quadratures, on the one hand, and between orthogonal Stieltjes eigenfunctions and generalized Gaussian quadratures on the other, is emphasized. Since the generalized Gaussian quadrature points are sure to appear where the density is large, the corresponding $n$th-order orthogonal Stieltjes eigenfunctions provide an optimal $L^2$ representation of the spectrum; i.e., they are the natural pseudostates of the system.[10] Similarly, the $n$th-order orthogonal Tchebycheff eigenfunctions provide an optimal $L^2$ spectral representation subject to the proviso that one eigenstate appear at a preselected energy. Although Eqs. (22), (28), and (29) include all the Stieltjes-Tchebycheff functions of order $n$ as $\epsilon$ is varied over the full spectral interval, it is useful to recognize the special natures and properties of the orthogonal Stieltjes and Tchebycheff eigenfunctions.

## III. COMPUTATIONAL APPLICATIONS

In this section, the Stieltjes-Tchebycheff development is applied to construction of the discrete and continuum (dipole) Schrödinger states of hydrogen atoms and molecules. In the former case, the Lanczos functions and polynomial recurrence coefficients required to construct $1s \rightarrow np/kp$ spectra are obtained in closed form. Detailed comparisons are made of the resulting Stieltjes-Tchebycheff functions with the correct regular Coulomb $p$ waves.[20] The static-exchange approximation is employed for body-frame calculations in molecular hydrogen to illustrate the computational requirements that arise in molecular applications. Large Gaussian basis sets and canonical orthogonalization methods are used in this case to construct the necessary Lanczos functions. The resulting Stieltjes-Tchebycheff orbitals are presented in three-dimensional graphical forms to clarify the natures of the continuum $k\sigma_u$ and $k\pi_u$ states, and the electronic dipole matrix elements are combined with appropriate Franck-Condon factors in construction of photoelectron spectra and vibrationally resolved and summed photoionization cross sections.

### A. Atomic hydrogen

For the regular $p$-wave spectrum in atomic hydrogen, Eqs. (9) and (10) can be solved in closed form using the complete discrete set of Laguerre functions of order $n+l+1/2l+2$ with constant exponent.[27] The matrix elements or polynomial recurrence coefficients $\alpha_j$ and $\beta_j$ of Eqs. (9), (10), (13), and (14) take the simple analytical forms[23]

$$\alpha_j = (j+1)/j \ , \tag{36a}$$

$$\beta_j = \tfrac{1}{2}[(j+3)/(j+1)]^{1/2} \ . \tag{36b}$$

These coefficients are seen to approach finite values in the limit $j \rightarrow \infty$, in accordance with the existence of an infinite set of convergent (reciprocal) power moments [Eqs. (7) and (33)] in this case.[23] By contrast, the positive-integer power moments of the density $g(\epsilon)$ of Eq. (3) are known to diverge for $k \geq 3$.[28] Consequently, use of the Hamiltonian $H$ in Eqs. (9) and (10), rather than $A(H)$, results in an invalid Lanczos problem, related to the divergence of the norms of the Cauchy functions of Eq. (7) and the consequent failure of Hilbert-space techniques. Such developments, although they can always be implemented numerically in finite basis sets, will generally not converge to the correct Schrödinger states.

In Figs. 1(a) and 1(b) are shown the first 20 Lanczos functions $rv_j(r)$ of Eqs. (9) and (10) for the $p$-wave spec-

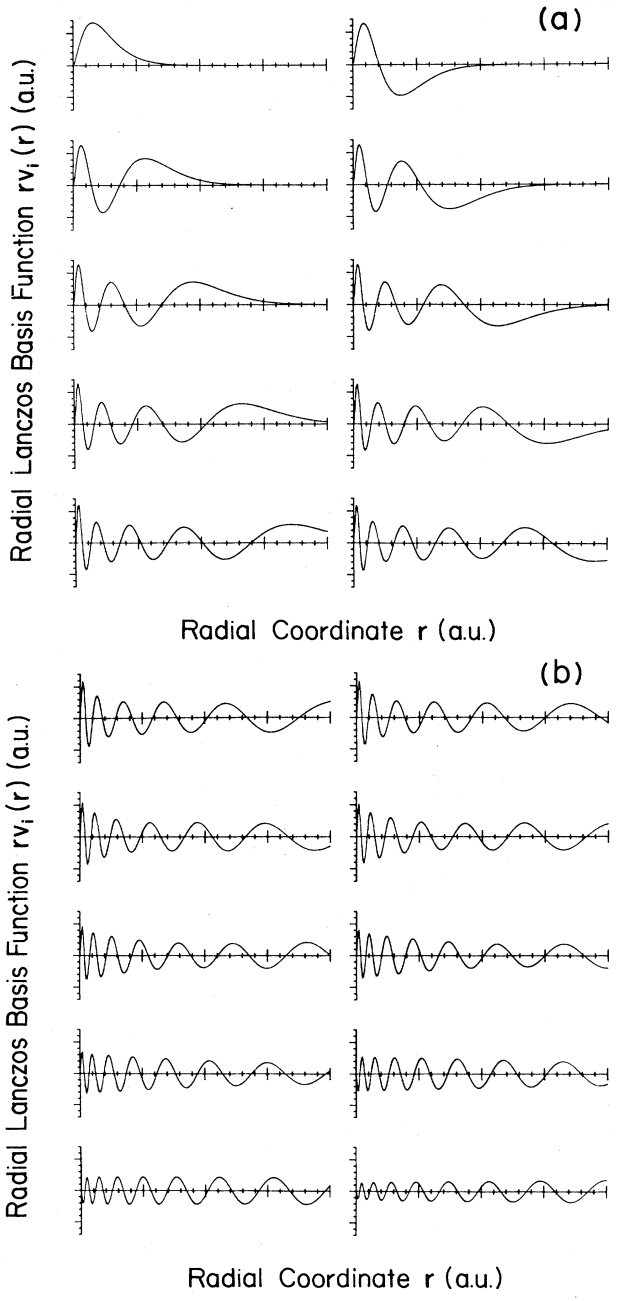


FIG. 1. (a) Lanczos functions $rv_j(r)$ of Eqs. (9) and (10) for dipole excitation of ground-state atomic hydrogen ($j=1-10$), constructed as discussed in the text. Abscissa spans $24a_0$, the ordinate 0.07 a.u. (b) As in (a) for $j=11-20$.

trum in atomic hydrogen. Starting with the defining test function $v_1(r)\sim re^{-r}$, these are seen to span increasingly larger portions of the spatial interval shown ($0-24a_0$). Moreover, since their nodes continue to change position with increasing $j$, in contrast to the behaviors of the familiar hydrogenic discrete states,[20] they remain linearly independent with increasing order, and can achieve completeness in finite orders over local portions of the spatial interval. Although the first 20 corresponding Cauchy functions (not shown) of Eq. (5) are linearly independent, they do not exhibit the nodal structures of the Lanczos functions of Figs. 1(a) and 1(b), since they are not an orthonormal set. As a consequence, the higher-order Cauchy functions include information already provided by the lower-order functions, and the associated higher-order spectral moments provide new information regarding the spectrum only in very high significant figures. This circumstance results in a numerically unstable eigenvalue problem when the Cauchy functions are employed directly as a basis set, and in a correspondingly unstable power moment problem [Eq. (34)].[10] These instabilities are avoided entirely through use of the Lanczos basis, corresponding recurrence coefficients $\alpha_j$ and $\beta_j$, and recursive solution of the moment problem.

The Lanczos functions of Figs. 1(a) and 1(b) and related recurrence coefficients [Eqs. (36)] are used to construct 20th-order Stieltjes functions in atomic hydrogen. These are the Stieltjes-Tchebycheff functions of 20th order [Eq. (22)] having energies at which the corresponding optical potential of Eqs. (19) to (21) vanishes identically. Consequently, their energies are the 20th-order generalized Gaussian quadrature points of the photoabsorption density, and their norms provide the corresponding quadrature weights [Eq. (35)]. In Fig. 2 are shown the first ten of the 20th-order Stieltjes functions that appear in the continuous spectrum. This figure indicates the correctly normalized 20th-order Stieltjes functions [Eqs. (29)] are converged to the correct corresponding regular Coulomb $p$ waves,[20] also shown in the figure, over the spatial interval

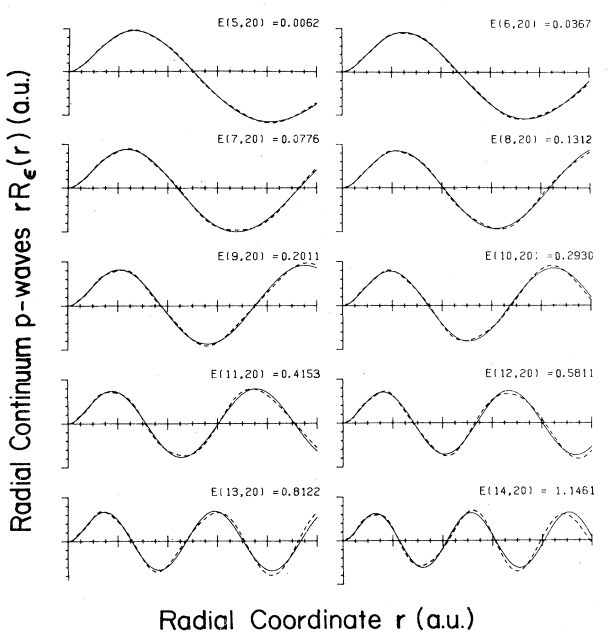


FIG. 2. Regular $p$ waves in atomic hydrogen, $rR_{\epsilon l}(r)$ ($l=1$); — — —, 20th-order Stieltjes eigenfunctions of Eqs. (29), constructed as discussed in the text; ——, correct values at the indicated [$E(i,20)$ a.u.] Stieltjes energies, constructed in accordance with Ref. 20. Ordinate spans 1 a.u., the abscissa $10a_0$.

indicated. Of course, for sufficiently large $r$ the Stieltjes functions decay, and do not reproduce the Coulomb $p$ waves. That is, the 20th-order Stieltjes functions are not eigenstates of $A(H)$ and $H$, but are spectrally broad.

The spectral content [Eq. (32)] of each of the ten functions of Fig. 2 is shown in Fig. 3. The Stieltjes energies, also shown in the figure, are seen to span the lower portion of the ionization spectrum in a sensible manner, in accordance with their Gaussian quadrature nature. That is, they appear in the spectrum where the density of Eq. (4), a monotonically decreasing function[20]

$$g(\epsilon)=\frac{8}{3}\frac{\exp[-4\epsilon^{-1/2}\tan^{-1}(\epsilon^{1/2})]}{(\epsilon+\frac{1}{2})^3[1-\exp(-2\pi\epsilon^{-1/2})]}\ , \qquad \epsilon(\text{a.u.})\geq 0 \quad (37)$$

also shown in the figure, is largest. Evidently, the lower-lying Stieltjes functions are spectrally narrower than are the higher-lying ones, in general accord with the observation that higher frequencies are required to reproduce correctly the high-energy Coulomb $p$ waves. The spectral interval shown is seen to be spanned fully by the ten Stieltjes functions of Fig. 2, with the spectral distribution of each state in Fig. 3 having a zero at the energies of the nine other states, in accordance with their orthogonality. Moreover, the (four) lower-lying 20th-order Stieltjes functions (not shown) are found to reproduce the $2p$, $3p$, and $4p$ states accurately, and to provide a fourth bound state corresponding to a spectral sum of all the other higher-lying discrete $np$ hydrogenic states. Finally, the remaining (six) 20th-order Stieltjes functions appear at higher energies in the continuous portion of the spectrum (not shown). Of these, the first four provide excellent approximations to the local portions of the corresponding regular $p$ waves, in spite of the fact that they are spectrally broad.

Stieltjes-Tchebycheff functions of various orders (10—100) and energies ($\epsilon\leq 5$ a.u.) are evaluated for the $p$-wave spectrum of atomic hydrogen. An overview of the results obtained appears in Fig. 4, where the weight function $\Gamma^{(n)}(\epsilon)$ or reciprocal norms of Eqs. (28) and (35) are shown for $n=10-100$. These evidently converge monotonically from above with increasing $n$ [Eq. (30)] to a spectrum that includes discrete features ($f$ numbers) at the appropriate Coulomb eigenvalues.[20] Above threshold in the essential spectrum ($\epsilon\geq 0$) the weights evidently decrease slowly but without limit, in accordance with the improper (infinite) normalization of the associated scattering states [Eq. (31)]. The points at which adjacent ($n$ and $n+1$) weight distributions touch give the $n$th-order Stieltjes energies. These points of coincidence are seen to form apparent rays with increasing $n$ that converge from above to the discrete Coulomb eigenvalues, in accordance with the Hylleraas-Undheim theorem. The $n$ Stieltjes energies of $n$th order provide $n+1$ intervals in which there appear one and only one of the $n+1$ Tchebycheff eigenvalues of $(n+1)$th order [Eq. (19)].[14] Consequently, as the energy variable $\epsilon$ is scanned over one of the Stieltjes intervals, the $n$ other Tchebycheff energies will correspondingly traverse the $n$ other Stieltjes intervals.[14] In this way a dense set of Stieltjes-Tchebycheff orbitals can be selected from the interval $(-\infty,+\infty)$. Alternatively, the entire interval can be spanned using a fine mesh, and Eq. (22) employed directly. The results of Fig. 4 are obtained by simply spacing 2000 points over the indicated energy interval.

In Fig. 5 are shown the weights $\Gamma^{(n)}(\epsilon)$ for $n=20-100$ employing a scale that presents more detail in the threshold region. It is seen that even the highest-order result ($n=100$) indicates the presence of only $\sim 10$ discrete states, as a consequence of the relatively weak contributions the higher $1s\rightarrow np$ Rydberg transitions in the hydrogen spectrum make to the discrete portion of the spectral density.[20] In this region of the spectrum, the Stieltjes-Tchebycheff weights correspond to an average over the infinite number of transition strengths that accumulate immediately below threshold, as well as to a portion of the

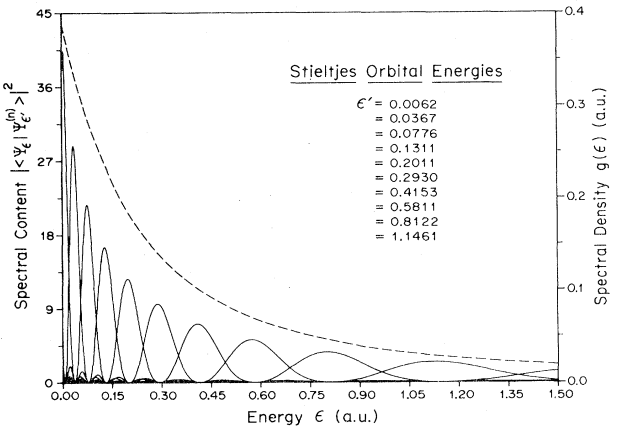


FIG. 3. Spectral content of Eq. (32) squared for the Stieltjes functions of Fig. 2, including the appropriate continuum normalization factors [Eq. (29)]; — — —, density function $g(\epsilon)$ of Eq. (37). 20th-order Stieltjes energies (a.u.) shown give the approximate line-shape centers.

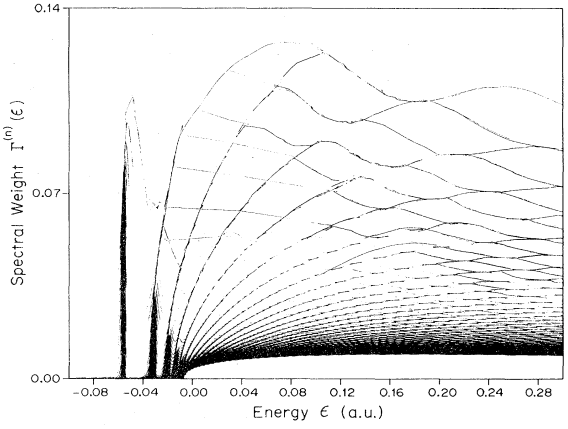


FIG. 4. Spectral weights $\Gamma^{(n)}(\epsilon)$ or reciprocal norms of Tchebycheff orbitals [Eqs. (28) and (35)] for $n=10-100$ for the $p$-wave spectrum in atomic hydrogen, constructed as discussed in the text. Note that the $1s\rightarrow 2p$ resonance at lower energy is not shown in the figure. All values in Hartree atomic units.

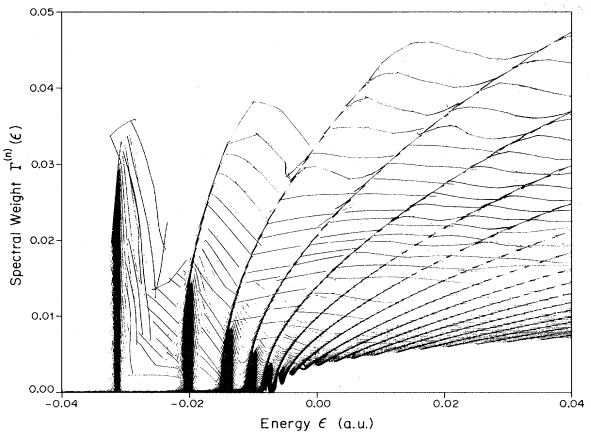


FIG. 5. As in Fig. 4, for $n=20-100$, showing more detail in the threshold region. Note that the $1s\rightarrow 2p$ and $3p$ resonances appear at lower energy and are not shown in the figure. All values in Hartree atomic units.

continuum transition strength above threshold.

The Stieltjes-Tchebycheff functions of Eqs. (28) and (29) corresponding to the weights of Figs. 4 and 5 are found to converge with increasing $n$ to the correct discrete $p$ states and regular $p$ waves in atomic hydrogen, respectively, in the appropriate energy intervals ($\epsilon<0$ and $\epsilon>0$). For $\epsilon<0$ but $\neq\epsilon_i$, convergence is obtained to highly oscillatory diverging states having improper (infinite) norm. Typical continuum results are shown in Figs. 6, 7, and 8, depicting Stieltjes-Tchebycheff functions for $\epsilon=0.5$, 2, and 5 a.u., respectively, for $n=10-80$ in steps of 10.

The correctly normalized Stieltjes-Tchebycheff functions of Fig. 6 are seen to converge with increasing $n$ to the correct regular Coulomb $p$ wave for $\epsilon=0.5$ a.u. also shown in the figure. In accordance with the spatial characteristics of the Lanczos functions [Figs. 1(a) and 1(b)], the Stieltjes-Tchebycheff functions are seen to converge first at smaller $r$ values, although for sufficiently large $n$ there is convergence over the full spatial interval shown (0—10 a.u.). Somewhat slower convergence is achieved for the higher energy states at $\epsilon=2$ and 5 a.u. shown in Figs. 7 and 8, respectively. Nevertheless, with increasing $n$ the correctly normalized Coulomb $p$ waves at both energies are seen to be reproduced by the Stieltjes-Tchebycheff functions over the spatial interval shown. Results similar to those shown in Figs. 6—8 are also obtained from the development for the regular $p$ waves in hydrogen at other energies in the interval $0\leq\epsilon<5$ a.u., and for higher energies as well, but with somewhat slower convergence achieved in the latter case. As indicated above, Eqs. (28) and (29) provide particularly convenient expressions for construction of Schrödinger states once the Lanczos functions are evaluated, since only the recursive relation of Eq. (14) is required to evaluate the necessary polynomials at the energy of interest.

In Fig. 9 are shown the spectral distributions [Eq. (32)] of some of the functions of Fig. 7 [$n=10$, 50, and 80], including the appropriate spectral density factors required for correctly normalized functions. The lowest order ($n=10$) result is seen to be relatively broad, although convergence to a $\delta$-function-like structure is evidently obtained with increasing order. As in Fig. 3, the zeros of the spectral distributions of Fig. 9 correspond to Radau quadrature points [Eq. (34)], which are the eigenvalues of Eqs. (19) and (25). Somewhat more rapid convergence than is shown in Fig. 9 is obtained to $\delta$-function-like structures for the lower-energy Stieltjes-Tchebycheff functions of Fig. 6, whereas for the higher-energy functions of Fig. 8, the convergence is slower. In all cases considered ($\epsilon\leq 5$ a.u.), however, the inner portions of the scattering functions are converged to the correct Coulomb results, in spite of their spectral widths.

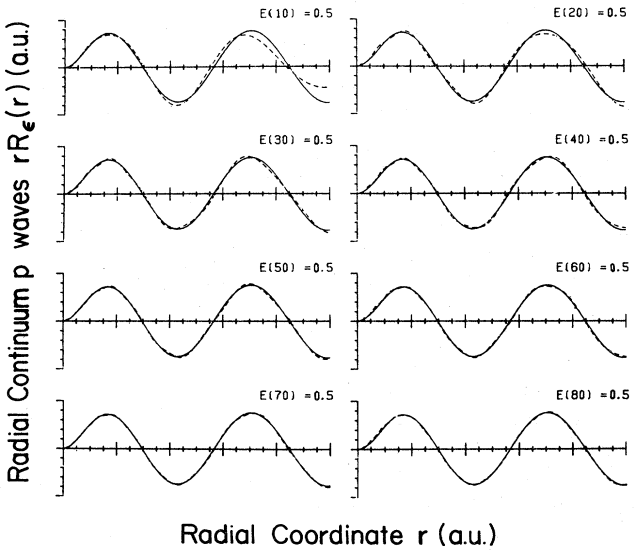


FIG. 6. Regular $p$ waves $rR_{\epsilon l}(r)$ ($\epsilon=0.5$ a.u., $l=1$) in atomic hydrogen; — — —, correctly normalized Stieltjes-Tchebycheff functions [Eq. (29)] for the indicated orders $E(n)$, constructed as discussed in the text; ——, correct results constructed in accordance with Ref. 20. Absissca spans $10a_0$, the ordinate 1 a.u.

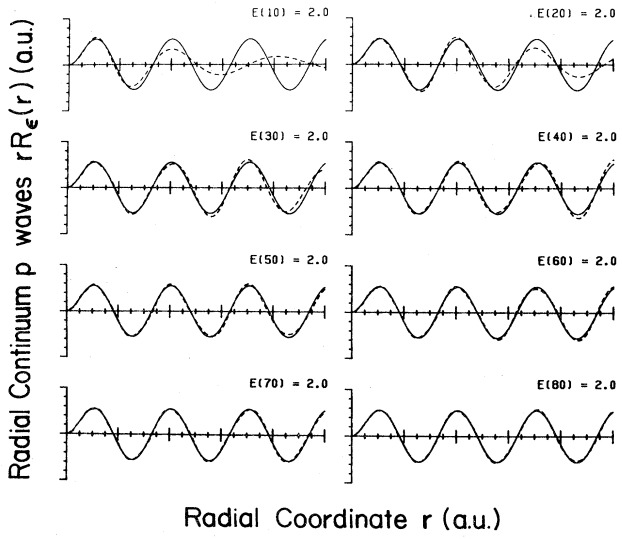


FIG. 7. As in Fig. 6, for $\epsilon=2$ a.u.

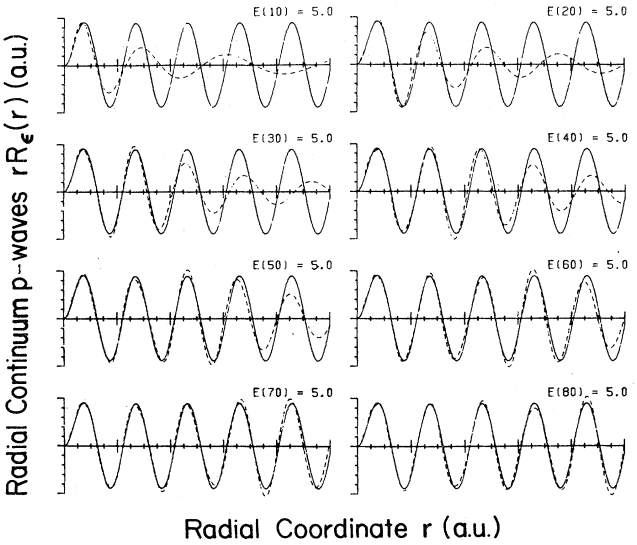


FIG. 8. As in Fig. 6, for $\epsilon=5$ a.u.

In addition to the regular $p$-wave results presented here, $l$-wave spectra in atomic hydrogen for $l \leq 15$ have also been evaluated employing the Stieltjes-Tchebycheff development with appropriate test functions $[\Phi \sim r^l P_l(\cos\theta)\Psi_0]$.[29] Pointwise convergence to the appropriate discrete and regular scattering states similar to the $p$ waves results presented here is also obtained in these cases. It should be noted that no particular difficulties are encountered in the present development from the Coulomb potential treated. Indeed, incorporation of the appropriate boundary conditions at the origin in the Lanczos basis is sufficient to ensure that the Stieltjes-Tchebycheff functions have the correct asymptotic behavior at large $r$, from which the Coulomb phase shifts can be determined, if required. Moreover, a second linearly independent solution can be constructed at any energy from the Stieltjes-Tchebycheff development by simply employing a Lanczos basis with "irregular" behavior at the origin, cutoff with a suitable function to ensure integral convergence. Alternatively, the regular Lanczos basis can be employed with the $q_j(\epsilon)$ replaced by (numerator) polynomials of the second kind $p_j(\epsilon)$ satisfying Eq. (14),

$$\beta_j p_{j+1}(\epsilon)=[a(\epsilon)-\alpha_j]p_j(\epsilon)-\beta_{j-1}p_{j-1}(\epsilon)\ , \tag{38}$$

but with the initial conditions $p_1=0$, $p_2=1/\beta_1$.[24] The corresponding Stieltjes-Tchebycheff functions

$$\chi_\epsilon^{(n)}=\sum_{j=1}^{n} p_j(\epsilon)v_j \tag{39}$$

are linearly independent of the $\Phi_\epsilon^{(n)}$ of Eq. (22). In the limit of large $n$, they correspond to solutions of an inhomogeneous Schrödinger equation with the test function $\Phi$ providing the inhomogeneity. Although the $\chi_\epsilon^{(n)}$ do not behave asymptotically as the irregular Coulomb functions, a linear combination of these and the $\Phi_\epsilon^{(n)}$ can always be constructed orthogonal to the $\Phi_\epsilon^{(n)}$ that does have the correct irregular asymptotic ($r\rightarrow\infty$) behavior. Since these are not required in the present development, they are not reported here.

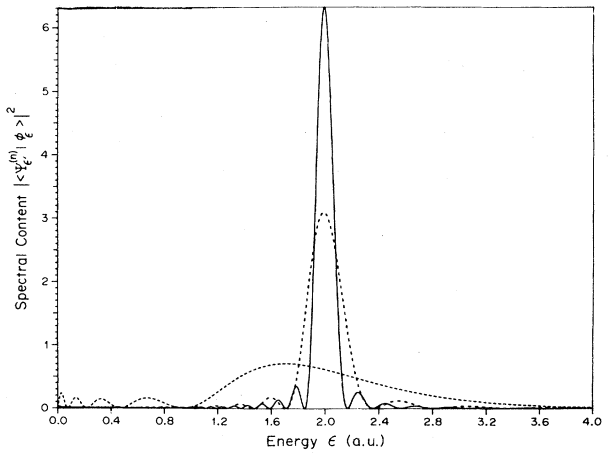


FIG. 9. Spectral content of Eq. (32) squared for the Stieltjes-Tchebycheff functions of Fig. 7 ($\epsilon=2$ a.u.), including the appropriate normalization factors [Eq. (29)]; $\cdots$, $n=10$; — — —, $n=50$; ——, $n=80$. Hartree atomic units are employed.

### B. Molecular hydrogen

In order to illustrate the computational requirements that arise in applications of the Stieltjes-Tchebycheff development to molecules, results are presented here for molecular hydrogen. To keep the development simple, computations are made in the Born-Oppenheimer, vertical-electronic, static-exchange approximation. In this approximation the photoabsorption cross section is obtained from body-fixed $1\sigma_g \rightarrow n\sigma_u/k\sigma_u$ and $n\sigma_u/k\pi_u$ excitations, and appropriate Franck-Condon and London-Hönl factors.[30] The $k\sigma_u$ and $k\pi_u$ scattering functions obtained from the Stieltjes-Tchebycheff development are presented in three-dimensional graphical forms. Although there have been numerous theoretical studies of photoionization in $H_2$,[31–46] the appropriate scattering functions have apparently not been reported explicitly in the literature.[9] Those presented here are seen to provide useful diagnostics of the scattering continua, and, in particular, to clarify the nature of the $\sigma\rightarrow\sigma^*$ transition in $H_2$.

Large Cartesian Gaussian basis sets $\{\phi_i;\ i=1$ to $N\simeq 150\}$ are employed to construct the ground-state $1\sigma_g$ orbital at $R_e$, and to solve the Lanczos equations in $\sigma_u$ and $\pi_u$ symmetry in the static-exchange or single-excitation configuration-mixing approximation.[8] In Table I are shown the supplemental functions employed, in addition to a standard $(4s,3p)/[3s,1p]$ valence basis,[47] in the calculations in $H_2$. These functions are chosen in accordance with the frequencies of the bound and scattering states expected, and on the basis of information derived from a previously reported preliminary study of the $H_2$ ionization spectrum.[9] To avoid the numerical difficulties that can arise from near linear dependence in such large basis sets, the overlap matrix

$$(\underline{S})_{ij}=\langle\phi_i\,|\,\phi_j\rangle \tag{40}$$

TABLE I. Supplemental Gaussian basis functions employed, in addition to the $(4s,3p)/[3s,1p]$ valence basis, in molecular hydrogen calculations.

| Location $[R_i$ (a.u.)][a] | Type | Exponents |
|---|---|---|
| 0.0 (c.m.) | $p_x,p_z$ | 0.200 |
| | | 0.100 |
| | | 0.050 |
| | | 0.025 |
| | | 0.0125 |
| | | 0.006 25 |
| | | 0.003 125 |
| | | 0.0010 |
| | | 0.0005 |
| | | 0.0002 |
| $\pm 0.70(R_e/2)$ | $s$ | 0.015 69 |
| | | 0.006 63 |
| | | 0.002 76 |
| | | 0.001 00 |
| | $p_x,p_z$ | 0.0933 |
| | | 0.0280 |
| | | 0.0140 |
| | | 0.0070 |
| $\pm 1.3$ and $\pm 2.8$ | $s,p_x,p_z$ | 2.0 |
| | | 1.0 |
| | | 0.5 |
| | | 0.2 |
| $\pm 4.3$ | $s,p_x,p_z$ | 1.0 |
| | | 0.5 |
| | | 0.2 |
| | | 0.1 |
| | $p_x,p_z$ | 2.00 |
| | | 0.05 |
| | | 0.02 |
| | | 0.01 |
| | | 0.005 |
| | | 0.002 |

[a]All functions are located at centers on the internuclear line at the indicated positions.

is constructed and diagonalized. Those linear combinations of basis functions that correspond to very small diagonal elements ($\lesssim 10^{-6}$) are discarded, and the remaining $M$-term ($M<N$) canonical basis set used to construct the ground-state Fock matrix. This matrix is first brought to self-consistency in the $(4s,3p)/[3s,1p]$ valence basis and then constructed and diagonalized in the full basis, providing a $1\sigma_g$ Fock orbital with energy of $-16.1286$ eV, as compared with an experimental vertical ionization potential of $\sim 16.0$ eV.[48] Next, the static-exchange Hamiltonian matrices are constructed in the $\sigma_u$ and $\pi_u$ subspaces of the $M$-term canonical basis set, and these are diagonalized. The resulting orthonormal static-exchange pseudospectra are then used in solving the Lanczos equations in each case. Since the static-exchange Hamiltonian is diagonal in these basis sets, there is no difficulty in constructing the matrix $\underline{A}(H)$ of Eqs. (6) and (9). It should be noted, consequently, that the Lanczos basis is not being used to diagonalize a matrix in the present development, since the static-exchange matrix is already diagonal. Rather, an $n$-term Lanczos basis, constructed in a larger $M$-term canonical static-exchange pseudostate basis is employed in constructing accurate approximations to the Stieltjes-Tchebycheff functions of Sec. II, in this case in the static-exchange approximation. In the present development, in which $\sim 40$ term pseudospectra are obtained, it is found that converged wave functions are obtained for $n \lesssim 10$. These observations are discussed in further detail below.

In Table II are shown the calculated values of the recurrence coefficients for both $\sigma_u$ and $\pi_u$ symmetry in $H_2$ obtained in the static-exchange approximation. These coefficients are seen to approach the correct asymptotic values also shown in the table with increasing $n$ up to $\cong 10$. The small oscillations in the coefficients in this interval ($1 \leq n \lesssim 10$) are a consequence of the presence of both discrete and continuum states in the spectrum.[23] For $n \gtrsim 10$ some of the coefficients are more irregular, exhibiting larger oscillations about the asymptotic values. These observations suggest the discrete pseudospectrum employed in the solution of the Lanczos equations begins to show through above 10th order, suggesting that valid results can be obtained in the basis sets employed for $n \lesssim 10$. This estimate is further verified in the immediately following discussion.

In Figs. 10(a) and 10(b) are shown the weight functions or reciprocal norms for $n=5-10$ of Eqs. (28) and (35) for $1\sigma_g \rightarrow k\sigma_u$ and $k\pi_u$ spectra in $H_2$. Not shown are the vertical-electronic, static-exchange approximations to the $X\,^1\Sigma_g^+ \rightarrow (2p\sigma_u)B\,^1\Sigma_u^+$ and $(2p\pi_u)C\,^1\Pi_u$ resonance transitions in each ($z$ and $x$ or $y$) polarization, which both appear at energies well below the ionization threshold.[30] Since the $f$ numbers for these transitions are relatively large ($\sim 0.3$), they dominate the discrete spectral region, and the 10th-order weight distributions are converged to sharp peaks at these energies. The second Rydberg transi-

TABLE II. Dipole recurrence coefficients for $1\sigma_g \rightarrow k\sigma_u$ and $k\pi_u$ spectra in $H_2$ in the static-exchange approximation. Values, in Hartree atomic units, are obtained from the Lanczos development of Eqs. (9) and (10) in the static-exchange approximation.

| | $1\sigma_g \rightarrow k\sigma_u$ spectrum | | $1\sigma_g \rightarrow k\pi_u$ spectrum | |
|---|---|---|---|---|
| | $\alpha_n$ | $\beta_n$ | $\alpha_n$ | $\beta_n$ |
| 1 | 1.6866 | 0.4653 | 1.3979 | 0.5434 |
| 2 | 1.3433 | 0.4994 | 1.2332 | 0.5150 |
| 3 | 1.0615 | 0.5471 | 1.1259 | 0.5022 |
| 4 | 0.9498 | 0.5038 | 1.0356 | 0.4879 |
| 5 | 1.0226 | 0.4494 | 1.0094 | 0.4729 |
| 6 | 1.0289 | 0.4554 | 0.9765 | 0.4732 |
| 7 | 0.9593 | 0.4781 | 0.9445 | 0.4798 |
| 8 | 0.8785 | 0.4612 | 0.9330 | 0.4348 |
| 9 | 1.0524 | 0.4026 | 0.9194 | 0.4893 |
| 10 | 0.8133 | 0.4958 | 1.1094 | 0.2404 |
| 11 | 1.1038 | 0.3482 | 0.9073 | 0.6634 |
| 12 | 0.8466 | 0.4700 | 0.9765 | 0.2358 |
| 13 | 0.8790 | 0.4804 | 0.7730 | 0.4891 |
| 14 | 1.0595 | 0.3520 | 1.0802 | 0.4725 |
| 15 | 0.9230 | 0.3712 | 0.9013 | 0.3613 |
| $\infty$[a] | 0.8436 | 0.4218 | 0.8436 | 0.4218 |

[a]Asymptotic values obtained from the expressions (Ref. 23) $\alpha_\infty = 1/(2\epsilon_t)$, $\beta_\infty = 1/(4\epsilon_t)$, where $\epsilon_t = 0.5927$ a.u. is the Koopmans ionization potential.

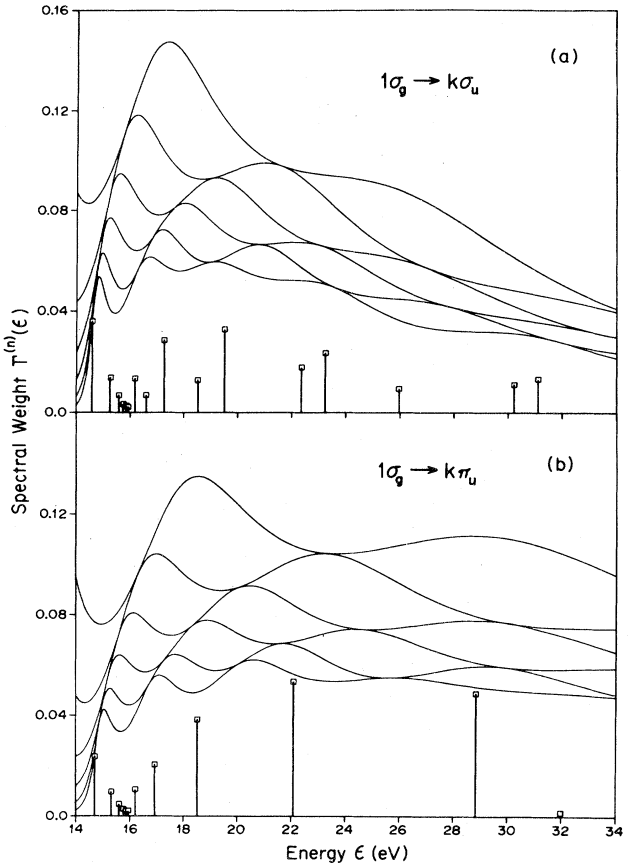


FIG. 10. (a) Spectral weights $\Gamma^{(n)}(\epsilon)$ or reciprocal norms of Stieltjes-Tchebycheff functions [Eqs. (28) and (35), $n=5-10$] for the $1\sigma_g \rightarrow k\sigma_u$ spectrum in $H_2$, constructed in the static-exchange approximation as discussed in the text. The $1\sigma_g \rightarrow 2p\sigma_u$ resonance transition appears at lower energy, and is not included in the figure. Vertical lines shown depict the primitive static-exchange pseudospectrum. (b) As in (a), for the $1\sigma_g \rightarrow k\pi_u$ spectrum in $H_2$. In this case the $1\sigma_g \rightarrow 2p\pi_u$ resonance is not shown.

tions $1\sigma_g \rightarrow 3p\sigma_u$ and $3p\pi_u$ have relatively weak $f$ numbers ($\sim 0.05$), and are barely discernible as discrete states in the two spectra. Above threshold, there are small waves present in both results of Fig. 10 due to the required coincidence of adjacent distributions at the Stieltjes energies. Although some of the higher-order ($10 < n \leq 15$) weight distributions obtained are satisfactory (not shown), with increasing $n$ the results show more pronounced waves that are unrelated to the coincidence of adjacent distributions, revealing the presence of the underlying discrete basis set and corresponding pseudospectral weight distributions, also shown in the figures. When $n = M$, the completely discrete pseudospectral weight distribution obtained from the basis-set static-exchange calculations is reproduced by the results of Eqs. (28) and (35). In this case, the Stieltjes-Tchebycheff development no longer provides useful wave functions at arbitrary ionization energies, although approximate wave functions are given by the pseudospectrum itself. Evidently, results up to $n = 10$ can be expected to provide converged Stieltjes-Tchebycheff functions in the present case. It is clear that Table II and Fig. 10 provide general means for assessing the extent of convergence of the Lanczos basis set and corresponding polynomial recurrence coefficients. In the following, Stieltjes-Tchebycheff functions up to 10th order are employed as diagnostics of the $1\sigma_g \rightarrow k\sigma_u$ and $k\pi_u$ cross sections in $H_2$.

In Figs. 11(a) and 11(b) are shown generalized or momentum-transfer-dependent cross sections

$$\sigma(\epsilon,q) = 4(\epsilon-\epsilon_0)\,|\,\langle k\phi_\epsilon\,|\,q^{-1}e^{i\vec{q}\cdot\vec{r}}\,|\,1\sigma_g\rangle\,|^2 \qquad (41)$$

for $1\sigma_g \rightarrow k\phi_\epsilon$ ($=k\sigma_u, k\pi_u$) ionization in $H_2$, obtained employing 10th-order Stieltjes-Tchebycheff approximations [Eq. (29)] to the required scattering functions. These correspond to first Born inelastic scattering cross sections when appropriate kinematical factors are included.[29] For present purposes, they constitute somewhat more general and sensitive probes of the scattering functions than do the dipole results, to which they reduce in the limit $q \rightarrow 0$. It should be noted that the vector $\underline{q}$ has been fixed along the lab frame $z$ axis and the results of Fig. 11 obtained by angle averaging Eq. (41) over all (equally weighted) orientations of the internuclear line. Evidently, the $q=0$ results of Figs. 11(a) and 11(b) are highly similar, although the $1\sigma_g \rightarrow k\pi_u$ cross section is somewhat smaller than the $1\sigma_g \rightarrow k\sigma_u$ result near threshold. This small difference at $q=0$ becomes fractionally larger with increasing $q$ as a consequence of the different portions of the continuum functions $k\phi_\epsilon$ the momentum-transfer dependent operator of Eq. (41) samples. Moreover, the $1\sigma_g \rightarrow k\sigma_u$ cross sections for higher $q$ exhibit more well-defined and larger maxima at low energy ($\epsilon \lesssim 25$ eV) than do the corresponding $1\sigma_g \rightarrow k\pi_u$ results. The behaviors of the cross sections

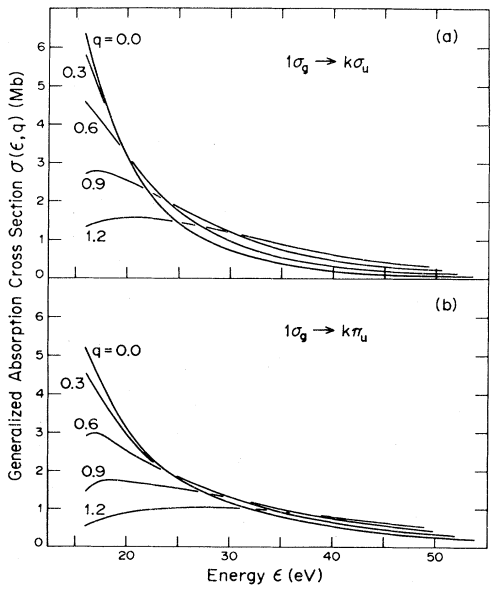


FIG. 11. (a) Momentum-transfer-dependent $1\sigma_g \rightarrow k\sigma_u$ ionization cross section in $H_2$ of Eq. (41), constructed in the static-exchange approximation for the indicated $q$ values (a.u.) as discussed in the text. (b) As in (a), for $1\sigma_g \rightarrow k\pi_u$ ionization.

of Fig. 11 can be clarified by examining the spatial characteristics of the $k\sigma_u$ and $k\pi_u$ scattering orbitals, for which purpose the Stieltjes-Tchebycheff development is highly suitable. It should be noted that the $q=0$ results of Figs. 11(a) and 11(b) are in good accord with previously reported static-exchange calculations employing conventional single-center computational methods.[40–46]

In Figs. 12(a) and 12(b) are shown three-dimensional graphical representations of the $1\sigma_g$ orbital and 10th-order $k\sigma_u$ and $k\pi_u$ Stieltjes-Tchebycheff functions of Eq. (29) in planes containing the internuclear line at energies in 2-eV intervals starting near the ionization threshold. The internuclear line runs from left to right in Fig. 12(a), which is the polarization direction ($z$) for $1\sigma_g \rightarrow k\sigma_u$ ionization, whereas the $x$ axis runs from left to right in Fig. 12(b), corresponding to the polarization direction in this case. When viewed from this perspective, the $k\sigma_u$ and $k\pi_u$ scattering functions at equal energies are seen to be highly similar, although there is a noticeable difference in each case. Specifically, the $k\sigma_u$ Stieltjes-Tchebycheff functions of Fig. 12(a) include cusplike features at the nuclei that are absent from the $k\pi_u$ functions. These features arise from compact $1\sigma_u 1s$ or $\sigma^*$ contributions to the $k\sigma_u$ spectrum that are largely responsible for the differences between the $1\sigma_g \rightarrow k\sigma_u$ and $k\pi_u$ cross sections of Fig. 11. Since the exponential factor in Eq. (41) samples the inner spatial regions of the scattering orbitals with increasing $q$, in which region the two sets of orbitals are seen to differ, differences in the two cross sections of Fig. 11 become more apparent at higher $q$ values. Although the effect is noticeable, it is comparatively small due to the limited spatial extent of the $1\sigma_u 1s$ orbital in $H_2$. For similar reasons, the total electron scattering cross section in $H_2$ does not reveal the presence of a resonance due to the $\sigma^*$ orbital, although rotationally and vibrationally inelastic cross sections are affected.[49] By contrast, $\sigma^*$ orbitals arising from $2s$-$2p$ shells in other molecules are found to affect photoionization and electron scattering cross sections more significantly.[8,9,49]

An alternative clarification of the presence of $\sigma^*$ contributions to the $k\sigma_u$ spectrum in $H_2$ is obtained from Fig. 13, which shows ground-state potential curves for $H_2$ and $H_2^+$, and curves for the $(2p\sigma_u)B\,{}^1\Sigma_u^+$ and $(2p\pi_u)C\,{}^1\Pi_u$ states in $H_2$.[50] Also shown in the figure is the diabatic curve associated with the configurational-state function $(\sigma\sigma^*)\,{}^1\Sigma_u^+$, constructed using frozen $1\sigma_g 1s$ and $1\sigma_u 1s$ orbitals for $R \leq 2.0$ Å, and made to approach smoothly the $H + H^-$ ground state in the $R \rightarrow \infty$ limit.[51] The latter configurational state is seen to cross the ground-state $H_2$ Franck-Condon zone at $\sim 20-30$ eV, clarifying the larger maxima in the $1\sigma_g \rightarrow k\sigma_u$ cross sections of Fig. 11(a) in this interval than in the corresponding $1\sigma_g \rightarrow k\pi_u$ result, and substantiating the presence of $\sigma^*$ contributions to the $k\sigma_u$ functions of Fig. 12(a). Of course, this configurational state will blend into the continuum in the static-exchange calculation, accounting for the presence of $\sigma^*$ contributions to the $k\sigma_u$ orbitals of Fig. 12(a) over a wide energy range. It is also interesting to note that the non-Rydberg behavior of the $(2p\sigma_u)B\,{}^1\Sigma_u^+$ state at large $R$ can be attributed to the $\sigma\sigma^*$ configuration, which contributes to this state for $R \gtrsim 1.2$ Å,[52] as is evident from the figure. By contrast, this state is almost purely Rydberg at $R_e$,[9] as is the $(2p\pi_u)C\,{}^1\Pi_u$ state, which follows closely the $H_2^+$ ground-state potential for all $R$. The Rydberg natures of the discrete states in the $H_2$ static-exchange spectrum at $R_e$ are further verified by quantum-defect analysis, which

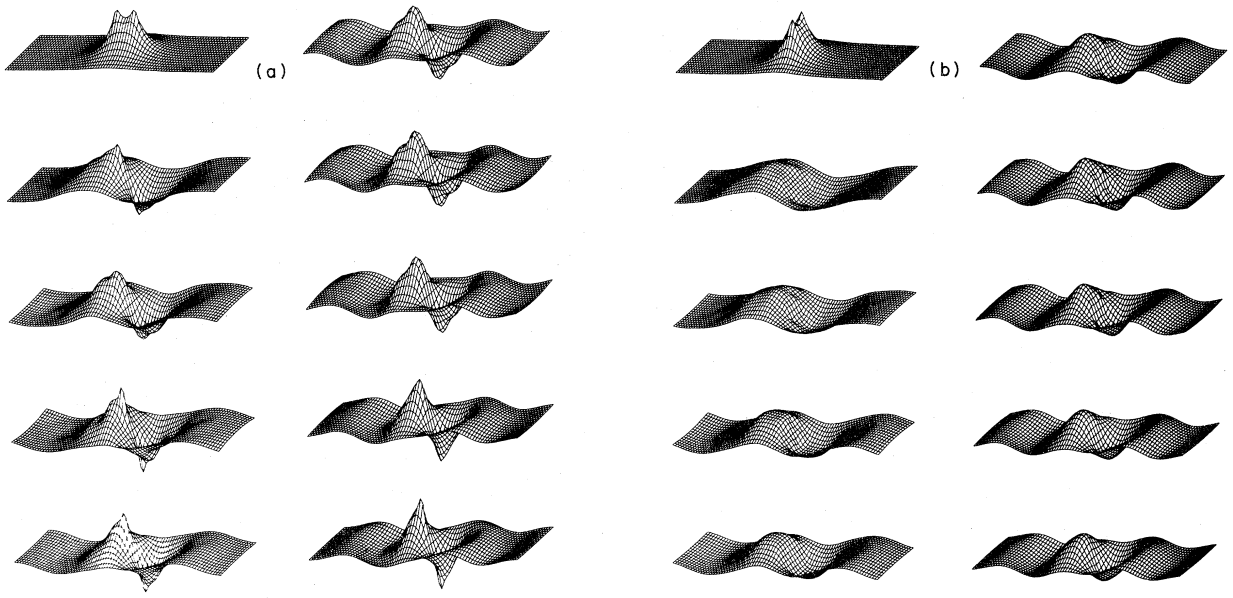


FIG. 12. (a) Occupied $1\sigma_g$ and 10th-order Stieltjes-Tchebycheff $k\sigma_u$ orbitals in $H_2$, the latter presented at 2-eV intervals beginning at 16 eV. Internuclear line runs from left to right in a rectangular box $\sim 16a_0$ long and $6a_0$ wide. (b) As in (a), for $k\pi_u$ orbitals, with the internuclear line rotated in the figure plane by 90°.

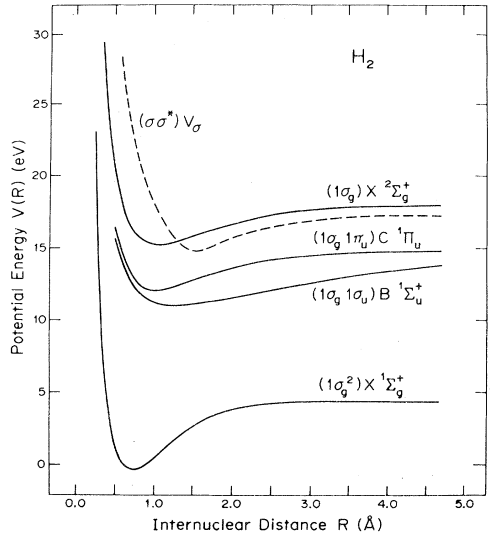


FIG. 13. Potential-energy curves in $H_2$ and $H_2^+$. $X\,^1\Sigma_g^+$, $B\,^1\Sigma_u^+$, $C\,^1\Pi_u$, and $X\,^2\Sigma_g^+$ curves are adopted from Ref. 50, whereas the $V_\sigma$ diabatic or $\sigma\sigma^*$ configurational-state curve is constructed from frozen compact orbitals as discussed in the text.

indicates the calculated vertical excitation energies follow closely the Rydberg formula with zero defects.

The electronic dipole cross sections ($q=0$) of Fig. 11 are combined in the present development with appropriate Franck-Condon factors[53] in construction of vibrationally resolved photoelectron spectra (PES) and photoionization cross sections. In Fig. 14 are shown calculated values in comparison with a recent high-resolution PES at 584 Å (=21.2 eV),[54] which evidently exhibits excitation of all the vibrational states in $H_2^+$. The theoretical values are constructed by regarding the cross sections of Fig. 11 as functions of kinetic energy, referring them to the experimental vibrational thresholds,[54] and multiplying by the appropriate Franck-Condon factors.[53] Moreover, experimental linewidths (~0.0124 eV)[54] and Gaussian line shapes are employed in constructing the theoretical results to facilitate comparison with experiment. In Table III are shown numerical values of the individual vibrational cross sections, corresponding to areas under the curves of Fig. 14. The experimental results shown in the table have been corrected for anisotropy and analyzer transmission effects, although the PES of Fig. 14 has not. Consequently, the latter should be regarded as a qualitative comparison, although the corrections are relatively small. Also shown in the table are the results of more elaborate calculations,[42] obtained employing vibrational averaging, correlated electronic wave functions, and previously described Stieltjes methods for constructing distributions and densities.[10] Evidently, the present results are in satisfactory accord with the measured values, and with the more elaborate theoretical results.

Because of the high degree of vibrational excitation achieved in the ionization of $H_2$, comparisons of vertical-electronic results with measured cross sections are generally invalid, particularly in the threshold region. In Fig. 15

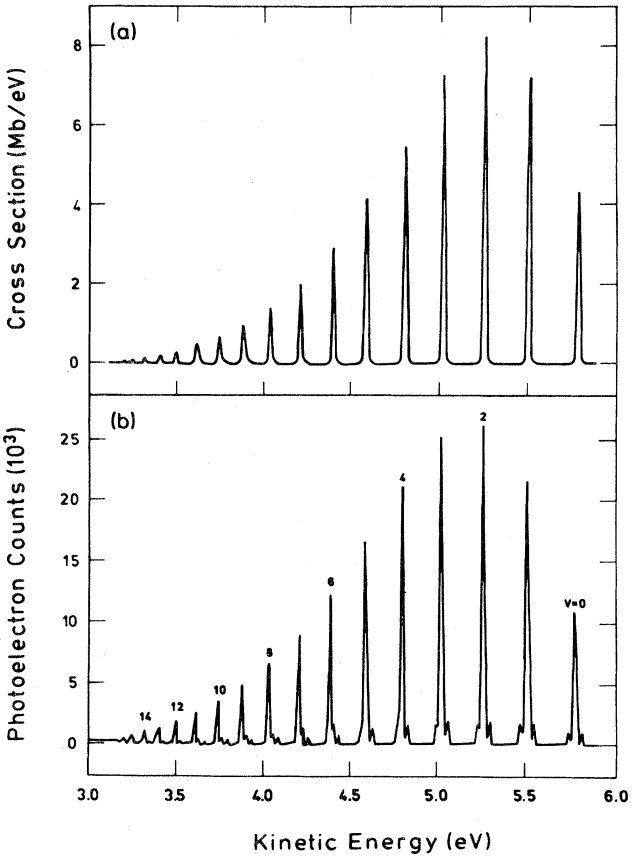


FIG. 14. Theoretical (a) and experimental (b) PES in $H_2$ at 21.2 eV (584 Å) incident photon energy. Theoretical values, in the static-exchange, Franck-Condon approximation, are constructed as discussed in the text. Experimental values (Ref. 54) shown are not corrected for anisotropy and analyzer transmission effects. Corresponding quantitative cross-sectional values are shown in Table III.

are shown experimental values for the $H_2$ photoionization cross section,[55–58] in comparison with the present results constructed from a sum over the individual vibrationally resolved cross sections. Evidently, the static-exchange Franck-Condon results of the present development are in generally good agreement with the measured values in $H_2$, although there is room for improvement. The previously reported calculations, including vibrational averaging and electronic correlation,[42] also shown in the figure, are evidently in very good quantitative accord with the measured values. It is satisfying that these results are also obtained employing previously described Stieltjes procedures for constructing distributions and densities,[10] suggesting the Stieltjes-Tchebycheff development can be expected to provide results equivalent or superior to conventional scattering calculations in a variety of computational approximations.

## IV. CONCLUDING REMARKS

Computational methods are reported for construction of discrete and continuum Schrödinger states in atoms

TABLE III. Vibrationally resolved photoionization cross sections in $H_2$ for 584-Å incident photons.

| $v'$ | Static exchange[a] | Correlated calculations[b] | Experimental values[c] |
|---|---|---|---|
| 0 | 0.6353 | 0.4533 | 0.477 ±0.006 |
| 1 | 1.1450 | 0.8639 | 0.907 ±0.008 |
| 2 | 1.3000 | 1.0036 | 1.048 ±0.008 |
| 3 | 1.1610 | 0.9313 | 0.975 ±0.007 |
| 4 | 0.9353 | 0.7656 | 0.793 ±0.006 |
| 5 | 0.7032 | 0.5866 | 0.598 ±0.005 |
| 6 | 0.5100 | 0.4315 | 0.446 ±0.004 |
| 7 | 0.3616 | 0.3105 | 0.315 ±0.004 |
| 8 | 0.2540 | 0.2211 | 0.223 ±0.003 |
| 9 | 0.1804 | 0.1568 | 0.157 ±0.003 |
| 10 | 0.1274 | 0.1113 | 0.1095±0.0007 |
| 11 | 0.090 90 | 0.079 27 | 0.0773±0.0005 |
| 12 | 0.064 89 | 0.056 59 | 0.0543±0.0005 |
| 13 | 0.046 40 | 0.040 38 | 0.0377±0.0011 |
| 14 | 0.033 04 | 0.028 56 | 0.0264±0.0003 |
| 15 | 0.022 99 | 0.019 69 | 0.0179±0.0002 |
| 16 | 0.015 03 | 0.012 73 | 0.0111±0.0002 |
| 17 | 0.008 316 | 0.006 933 | 0.0068±0.0002 |
| 18 | | 0.002 162 | |
| 19 | | 0.000 098 | |
| Total[d] | 7.595 | 6.083 | 6.280 |

[a]Present values obtained in the vertical-electronic, Franck-Condon, static-exchange approximation.
[b]Previous calculations including the effects of vibrational averaging and electronic correlation (Ref. 42), constructed from previously described Stieltjes methods for distributions and densities (Ref. 10).
[c]Experimental values corrected for anisotropy and analyzer effects (Ref. 54).
[d]Refers to the sum of the indicated vibrationally resolved cross sections. Units are Mb.

and molecules employing explicit Hilbert-space procedures familiar from bound-state studies. An $L^2$ Lanczos basis and associated orthogonal polynomials are seen to provide particularly simple and computationally convenient expressions for Schrödinger states at discrete or continuum energies. The resulting $n$th-order Stieltjes-Tchebycheff functions give accurate approximations to local portions of Schrödinger states, and are shown to provide exact optical-potential solutions of the full matrix Schrödinger equation in the complete Lanczos basis. The spectral compositions of these functions in finite orders are evaluated in closed form without explicit reference to or construction of the corresponding correct Schrödinger states. Use of a Lanczos basis ensures that Stieltjes-Tchebycheff functions correspond closely to previously described moment-theory approximations to spectral densities and distributions. Specifically, the energies at which the $n$th-order optical potential vanishes identically are seen to correspond to the generalized Gaussian quadrature points of the spectral density. The norms of the associated orthogonal Stieltjes eigenstates give the corresponding quadrature weights. Radau quadrature points are obtained from orthogonal Tchebycheff eigenstates that diagonalize the $n$th-order optical-potential problem, the norms of which give the corresponding Radau quadrature weights. Consequently, the Stieltjes-Tchebycheff functions provide information necessary for physical renormalization at any energy, in spite of the absence of a spatially asymptotic tail. Although Stieltjes-Tchebycheff functions at two arbitrary energies are not orthogonal, they are so in the limit of high order, in which case convergence to the correct Schrödinger states is achieved.

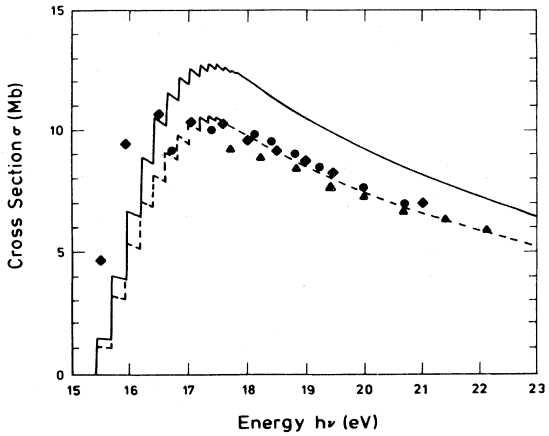


FIG. 15. Photoionization cross sections in $H_2$; ——, present results constructed from static-exchange cross sections of Figs. 11 ($q=0$) and appropriate Franck-Condon factors (Ref. 53); — — —, previous Stieltjes calculation including vibrational averaging and electronic correlation (Ref. 42). Experimental values: ●, Ref. 55; ▲, Ref. 57; ◆, Ref. 58.

The nature of the method and properties of Stieltjes-Tchebycheff functions are illustrated with detailed computational applications to hydrogen atoms and molecules. Closed-form results are presented for the $p$-wave spectrum in atomic hydrogen. The Stieltjes-Tchebycheff functions

are seen to exhibit pointwise convergence to the correct regular $p$ waves in this case, and it is indicated how irregular solutions can also be constructed. Correspondingly, in the case of molecular hydrogen Gaussian basis sets and canonical orthogonalization procedures are found to provide Lanczos and Stieltjes-Tchebycheff functions that give useful representations of the continuum states. In this way photoelectron spectra and related cross sections are obtained which are in good accord with corresponding measured values, and useful diagnostics are provided of the scattering wave functions.

Certain distinct advantages are inherent in the Stieltjes-Tchebycheff procedure for computational studies of Schrödinger spectra relative to conventional methods for separate construction of discrete and continuum wave functions. First, in addition to providing approximations of uniform quality to large portions of the spectrum from a unified computational procedure, some of the difficulties that have hampered conventional scattering calculations of molecular continuum states are avoided entirely by use of an explicit $L^2$ or Hilbert-space approach. Specifically, conventional single-center $l$-wave representations of scattering functions can be very slowly convergent, whereas the Stieltjes-Tchebycheff development makes full use of the multicenter nature of $L^2$ basis-set approaches. In order to take advantage of this opportunity, and to avoid the loss of spectral resolution a global approach might seem to entail, it is necessary to employ well-chosen sufficiently large basis sets and canonical orthogonalization procedures, as in the present studies. By contrast, some of the previously reported moment-theory calculations of photoabsorption cross sections employed smaller basis sets that are found to provide only low-order Stieltjes-Tchebycheff functions. Many of these earlier calculations have now been repeated in much larger basis sets, and higher-order Stieltjes-Tchebycheff functions constructed. These studies are topics of separate reports to be issued subsequently, which will clarify further the use of large basis sets in molecular spectral calculations.

Second, Stieltjes-Tchebycheff functions are easily Fourier analyzed, providing momentum wave functions for both bound and scattering states at all energies. Scattering states in momentum space provide information required for construction of the angular distributions of photoejected electrons. Since the explicit expressions obtained in this way, described in detail in separate reports, are relatively simple and well suited for both body- and laboratory-frame graphical representations, a significant degree of insight is obtained thereby into the nature and energy variation of molecular anisotropy factors. By contrast, $l$-wave representations of molecular anisotropy factors obtained from conventional scattering approaches are not well suited for developing physical insights.

Third, because of the very compact representation provided for single-channel functions by the Stieltjes-Tchebycheff development, it is possible to also perform coupled-channel calculations following a standard reaction-matrix formalism. Such calculations have been performed in selected diatomic and polyatomic molecules, studies that will be described in separate reports. By contrast, very few coupled-channel molecular photoionization calculations have been performed employing single-center $l$-wave representations due to the generally unmanageable dimensions of such problems.

Fourth, Stieltjes-Tchebycheff functions can be constructed for continuous values of the ionization energy, providing background scattering states suitable for autoionization, dissociative recombination, and related studies in which a quasidiscrete state merges with a continuum. Such topics are largely special cases of the general coupled-channel problem indicated above, but deserve separate mention in view of the general lack of a useful computational approach to such problems on the basis of conventional $l$-wave representation scattering theory.

Fifth, since Stieltjes-Tchebycheff functions are constructed in body-frame point group symmetry they provide a convenient diagnostic for the presence of compact resonancelike contributions to ionization continua. By contrast, $K$- or $S$-matrix normalized $l$-wave represented scattering functions provide a less suitable diagnostic. Moreover, body-frame eigenchannel functions, although of appropriate symmetry, can change spatial characteristics rapidly in the neighborhoods of resonances due to the familiar noncrossing rule for phase shifts, and consequently do not isolate such features in a single channel.

## ACKNOWLEDGMENTS

Computational assistance provided by D. J. Margoliash and K. Greenwald is gratefully acknowledged. These studies are supported by the Chemistry and International Programs Divisions of the National Science Foundation, by the U.S. National Aeronautics and Space Administration, and by the Petroleum Research Fund, administered by the American Chemical Society. It is a pleasure to thank Dr. G. H. F. Diercksen for his kind hospitality during portions of the course of these investigations.

---

*Address for correspondence.

[1]J. A. R. Samson, Phys. Rep. 28, 303 (1976).

[2]E. E. Koch and B. F. Sonntag, in *Synchrotron Radiation,* edited by C. Kunz (Springer, Berlin, 1979).

[3]C. E. Brion and A. Hamnett, Adv. Chem. Phys. 45, 2 (1981).

[4]J. Berkowitz, *Photoabsorption, Photoionization, and Photoelectron Spectroscopy* (Academic, New York, 1979).

[5]P. W. Langhoff, in *Proceedings of the NATO Advanced Study Institute on Methods in Computational Molecular Physics,* edited by G. H. F. Diercksen and S. Wilson (Reidel, Dordrecht, Holland, 1983), pp. 299–334.

[6]P. W. Langhoff, in *Theory and Applications of Moment Methods in Many-Fermion Systems,* edited by B. J. Dalton, S. M. Grimes, J. P. Vary, and S. A. Williams (Plenum, New York, 1980), pp. 191–212.

[7]P. W. Langhoff, in *Electron-Molecule and Photon-Molecule*

*Collisions,* edited by T. Rescigno, V. McKoy, and B. Schneider (Plenum, New York, 1979), pp. 183–224.
[8]P. W. Langhoff, N. Padial, G. Csanak, T. N. Rescigno, and B. V. McKoy, Int. J. Quantum Chem. S 14, 285 (1980); J. Chim. Phys. 77, 589 (1980).
[9]M. R. Hermann and P. W. Langhoff, Chem. Phys. Lett. 82, 242 (1981).
[10]P. W. Langhoff, Chem. Phys. Lett. 22, 60 (1973); P. W. Langhoff and C. T. Corcoran, J. Chem. Phys. 61, 146 (1974); P. W. Langhoff, J. S. Sims, and C. T. Corcoran, Phys. Rev. A 10, 829 (1974).
[11]N. F. Lane, Rev. Mod. Phys. 52, 29 (1980).
[12]J. C. Tully, R. S. Berry, and B. J. Dalton, Phys. Rev. 176, 95 (1968).
[13]P. W. Langhoff, in *Electron-Atom and Electron-Molecule Collisions,* edited by J. Hinze (Plenum, New York, 1983), pp. 297–314.
[14]C. T. Corcoran and P. W. Langhoff, J. Math. Phys. 18, 651 (1977).
[15]J. A. Shohat and J. D. Tamarkin, *The Problem of Moments,* 2nd ed. Mathematical Surveys (American Mathematical Society, Providence, R. I., 1950), Vol. 1.
[16]P.-O. Löwdin, Int. J. Quantum Chem. 21, 69 (1982).
[17]M. R. Hermann and P. W. Langhoff, Int. J. Quantum Chem. 23, 135 (1983).
[18]M. R. Hermann and P. W. Langhoff, J. Math. Phys. 24, 541 (1983).
[19]C. Lanczos, J. Res. Natl. Bur. Stand. 45, 255 (1950).
[20]H. A. Bethe and E. Salpeter, *Quantum Mechanics of One- and Two-Electron Atoms* (Academic, New York, 1957).
[21]P. W. Langhoff, Phys. Reps. (unpublished).
[22]S. T. Epstein, *The Variational Method in Quantum Chemistry* (Academic, New York, 1974).
[23]P. W. Langhoff, C. T. Corcoran, J. S. Sims, F. Weinhold, and R. M. Glover, Phys. Rev. A 14, 1042 (1976).
[24]N. I. Akhiezer, *The Classical Moment Problem* (Oliver and Boyd, London, 1965).
[25]H. S. Wall, *Analytic Theory of Continued Fractions* (Van Nostrand, New York, 1948).
[26]Yu V. Vorobyev, *Method of Moments in Applied Mathematics* (Gordon and Breach, New York 1965).
[27]H. Shull and P.-O. Löwdin, J. Chem. Phys. 23, 1362 (1955).
[28]P. W. Langhoff, J. Chem. Phys. 57, 2604 (1972).
[29]D. J. Margoliash and P. W. Langhoff, J. Comput. Phys. 49, 44 (1983); 49, 67 (1983).
[30]G. Herzberg, *Spectra of Diatomic Molecules,* 2nd ed. (Van Nostrand, New York, 1950).
[31]M. Shimizu, J. Phys. Soc. Jpn. 15, 1440 (1960).
[32]M. Shimizu, J. Phys. Soc. Jpn. 18, 811 (1963).
[33]M. R. Flannery and U. Öpik, Proc. Phys. Soc. London 86, 491 (1965).
[34]S. P. Khare, Phys. Rev. 173, 43 (1968).
[35]H. P. Kelly, Chem. Phys. Lett. 20, 547 (1973).
[36]Y. Itikawa, J. Electron Spectrosc. Relat. Phenom. 2, 125 (1973).
[37]P. H. S. Martin, T. N. Rescigno, V. McKoy, and W. H. Henneker, Chem. Phys. Lett. 29, 496 (1974).
[38]A. L. Ford, K. K. Docken, and A. Dalgarno, Astrophys. J 195, 819 (1975).
[39]F. Hirota, J. Electron Spectrosc. Relat. Phenom. 9, 148 (1976).
[40]C. M Dutta, F. M. Chapman, and E. F. Hayes, J. Chem. Phys. 67, 1904 (1977).
[41]H. Tai and M. R. Flannery, Phys. Rev. A 16, 1124 (1977).
[42]J. W. Davenport, Int. J. Quantum Chem., Symp. S11, 89 (1977).
[43]S. V. ONeil and W. P. Reinhardt, J. Chem. Phys. 69, 2126 (1978).
[44]Y. Itikawa, Chem. Phys. 30, 109 (1978).
[45]L. Y. C. Chiu and S. R. Samanta, J. Quant. Spectrosc. Radiat. Transfer 25, 253 (1981).
[46]G. Raseev and H. Le Rouzo, Phys. Rev. A 27, 268 (1983).
[47]T. H. Dunning and J. P. Hay, in *Modern Theoretical Chemistry,* edited by H. F. Schaefer III (Plenum, New York, 1976), Vol. 3, Chap. 1.
[48]D. W. Turner, C. Baker, A. K. Baker, and C. B. Brundle, *Molecular Photoionization Spectroscopy* (Wiley, New York, 1970).
[49]G. J. Schulz, Rev. Mod. Phys. 45, 423 (1973).
[50]T. E. Sharp, At. Data 2, 119 (1971).
[51]J. C. Slater, *Quantum Theory of Molecules and Solids* (McGraw-Hill, New York, 1963), Vol. I.
[52]R. S. Mulliken and W. C. Ermler, *Diatomic Molecules* (Academic, New York, 1977).
[53]S. Rothenberg and E. R. Davidson, J. Mol. Spectrosc. 22, 1 (1967).
[54]J. E. Pollard, D. J. Trevor, J. E. Reutt, Y. T. Lee, and D. A. Shirley, J. Chem. Phys. 77, 34 (1982); see also, L. Åsbrink, Chem. Phys. Lett. 7, 549 (1970).
[55]G. R. Cook and P. H. Metzger, J. Opt. Soc. Am. 54, 968 (1964).
[56]J. A. R. Samson and R. B. Cairns, J. Opt. Soc. Am. 55, 1035 (1965).
[57]L. C. Lee, R. W. Carlson, and D. L. Judge, J. Quant. Spectrosc. Radiat. Transfer 16, 873 (1976); see also, J. A. R. Samson and G. N. Haddad (unpublished) and J. W. Taylor and G. Marr (unpublished).
[58]C. Backx, G. R. Wight, and M. J. Van Der Wiel, J. Phys. B 9, 315 (1976).